Renewable Energy 256 (2026) 124193

Contents lists available at ScienceDirect

Renewable Energy

journal homepage: www.elsevier.com/locate/renene

# Designing off-grid hybrid renewable energy systems under uncertainty: A two-stage stochastic programming approach

Mattia Calabrese *, Andrea Ademollo, Carlo Carcasci

*University of Florence, Department of Industrial Engineering (DIEF), Via di Santa Marta, 3, 50139, Florence, Italy*

ARTICLE INFO

*Keywords:*
Hybrid renewable energy system
Renewable energy storage
Multi-objective optimization
Two-stage stochastic programming
Power-to-Hydrogen-to-Power

ABSTRACT

The decarbonization of remote energy systems presents both technical and economic challenges, due to their dependance on fossil fuels and the variability of renewable energy sources. This study introduces a Two-Stage Stochastic Programming approach to optimize Hybrid Renewable Energy Systems under uncertainty in renewable energy production. The methodology is applied to the island of Pantelleria, aiming to minimize Total Annualized Costs and $CO_2$ emissions using an ε-constraint approach. Results show that, within the set of optimized configurations, stricter $CO_2$ emissions constraints increase costs, due to the need for oversized components to ensure supply reliability. Nevertheless, even the zero-emissions scenario offers significant economic benefits compared to the current diesel-based system. Total Annualized Costs are reduced from 15.5 M€ to 8.10 M€ in the deterministic case and to 9.37 M€ in the stochastic one. The additional cost in the stochastic configuration is offset by improved reliability, ensuring demand is met under all scenarios. A sensitivity analysis on electricity demand reveals the necessity of further larger components, leading to a 27.0 % cost increase in a fully renewable scenario with stochastic optimization for a 10 % demand increase. These findings highlight the importance of stochastic optimization in designing cost-effective off-grid renewable energy systems.

## 1. Introduction

The decarbonization of the energy sector is a fundamental objective in the ongoing effort against climate change. Consequently, many nations are establishing ambitious targets for cutting Greenhouse Gas (GHG) emissions. In its recent report [1], the International Energy Agency (IEA) outlined a pathway to achieving net-zero by 2050, emphasizing the urgent need for a rapid transition towards renewable energy, electrification, and energy efficiency. The European Union (EU) committed to reducing emissions by at least 55 % by 2030, as part of its "Fit for 55" [2] initiative, with the ultimate goal of achieving full carbon neutrality by 2050. These targets are driving the energy transition, particularly in the power generation sector, which accounts for 42 % [3] of global energy-related carbon dioxide ($CO_2$) emissions.

Despite their relatively small contribution to global emissions, remote communities that lack connection to the electricity grid remain heavily dependent on fossil fuels, particularly with Diesel Generators (DG). This reliance results in significant energy costs - up to ten times the levels observed in the mainland [4] – and raises concerns regarding the security of energy supply. In fact, fuel prices are highly volatile, and transportation costs to remote locations further amply the financial burden. The growing interest in addressing these challenges is reflected in European initiatives, such as the European Commission's "Clean Energy for EU Islands" [5] program.

A significant number of studies have explored solutions to these issues. Among the proposed solutions, the hybridization of the energy system has shown potential in reducing the cost of energy. Malheiro et al. [6], for instance, demonstrated that in the absence of a backup DG system, the required Battery Energy Storage System (BESS) capacity would be three times larger, significantly increasing the Levelized Cost of Electricity (LCOE). On the other hand, Cai et al. [7] have shown that Hybrid Renewable Energy Systems (HRES) are considerably more cost-effective than a system reliant solely on DGs, as they reduce fuel consumption. Additionally, incorporating a Hydrogen Storage System (HSS) has been found to further reduce the LCOE [8]. Gray et al. [9] highlighted the advantages of HSS over BESS due to its absence of self-discharge and greater reliability. However, they also noted that the Power-to-Gas-to-Power (P2G2P) process in a hydrogen storage system still has a lower efficiency, particularly for short-term storage. Brinkhaus et al. [10] determined that while hydrogen is a viable option for

* Corresponding author.
*E-mail addresses:* mattia.calabrese@unifi.it (M. Calabrese), andrea.ademollo@unifi.it (A. Ademollo), carlo.carcasci@unifi.it (C. Carcasci).

https://doi.org/10.1016/j.renene.2025.124193
Received 3 April 2025; Received in revised form 7 August 2025; Accepted 7 August 2025
Available online 11 August 2025

long-term seasonal storage, batteries are more appropriate for short-term energy supply. Consequently, combining these two storage technologies enhances system reliability, making them well-suited for deployment in remote locations. Marocco et al. [11] showed that when there are no constraints on emissions, the most cost-effective configuration comprises Renewable Energy Sources (RESs), BESS, and DGs. However, as the reliance on fossil fuels decreases, hydrogen storage becomes crucial in preventing the oversizing of renewable energy capacity. Similar findings were reported by Marchenko et al. [12], who observed a 31.0 % reduction in system costs through the integration of hydrogen production and storage.

To determine the optimal energy mix, many studies have employed a Multi-Objective Optimization approach, which enables the simultaneous consideration of multiple and conflicting objectives. Common optimization goals in literature include minimizing system costs, such as LCOE [13] or annual costs [14], and reducing environmental impact, typically measured in terms of $CO_2$ emissions [15]. Optimization problems for HRES are generally addressed using meta-heuristic methods [16], such as Genetic Algorithms [17] and Particle Swarm Optimization [11], or through mathematical programming approaches, including Linear Programming (LP) [18] and Mixed Integer Linear Programming (MILP) [19].

Most previous studies had a deterministic approach to the optimization problem. Only a few works incorporated the uncertainties associated with HRES. However, these uncertainties are an intrinsic feature of such systems, and a deterministic approach may fail to accurately characterize the system. Dufo-Lopez et al. [20] for instance, proposed a stochastic optimization strategy based on the Monte Carlo (MC) method, which generates a Probability Density Function for the outcomes rather than a single deterministic value. Their methodology applied two Genetic Algorithms: one for component sizing and another for control strategy optimization. Moreover, Gong et al. [21] analyzed the flexible operation of hydropower and hydrogen systems to mitigate the variability of renewable sources. In their study, they evaluated the presence of a benefit loss when maintaining operational decisions within the flexible space during climate emergencies.

A particularly effective approach for addressing uncertainties in stand-alone energy systems is two-stage stochastic programming. This type of model introduces two groups of variables. First-stage variables are predetermined and maintain their value across all scenarios, regardless of variations in uncertain parameters. Conversely, second-stage variables are flexible and adjust dynamically in response to the actual realization of these uncertainties. A change in parameters, such as electrical load or RES production could make the system unable to completely fulfill the demand. Stochastic programming must ensure that the designed system (first-stage variables) is able to meet the demand in all potential scenarios by varying its operation (second-stage variables). Two-stage stochastic programming is used in many studies in the energy sector. Marzi et al. [22], for instance, proposed a two-stage stochastic approach to understand how the integration of seasonal storage through power-to-gas could add flexibility and help mitigate the impact of uncertainties in a multi-energy system. Moreover, Huang et al. [23] built a two-stage stochastic programming model to minimize the expected costs of a regional-scale electricity system under demand uncertainty.

In the present study, a two-stage stochastic multi-objective optimization problem is formulated within an LP framework to determine the optimal configuration and operation of an HRES. The system consists of photovoltaic (PV) panels, Wind Turbines (WT), DGs, HSS, and BESS. The proposed methodology is applied to Pantelleria island, located southwest of the Sicilian coastline in Italy. Pantelleria participates in both the "Clean Energy for EU Islands" [5] program and the "Smart Island" project [24]. The island currently relies principally on DGs, and its remote location makes grid connection unfeasible. Given the existence of numerous similar cases in the Mediterranean and remote European communities, the approach has significant replicability potential.

### 1.1. Scope of the present work

While numerous studies have focused on the optimization of hybrid renewable energy systems, a significant gap remains in their design under uncertainty. In stand-alone HRES, any variability – such as lower than predicted renewable generation or higher than expected demand – can result in an inability to supply the required energy to the end-user. This issue worsens when constraints are imposed on CO2 emissions, limiting the utilization of diesel generators as a flexible backup system. The major limitation in current research lies in the lack of systematic investigation into how uncertainties affect optimal component sizing and operational strategies. In these contexts, ignoring uncertainty can lead to under-dimensioned systems, misestimated costs, and potential reliability issues. To address these challenges, variability must be considered during the design process. However, to the best of the authors' knowledge, no research has systematically analyzed how uncertainties impact the optimal sizing and operation of off-grid HRES.

In this study, a cost-emissions Pareto front is initially obtained using a deterministic approach. Subsequently, the two-stage stochastic programming framework is applied to evaluate how uncertainty in renewable energy availability influences system configuration, components' operation, and associated costs. The same analysis is conducted varying the electricity demand to assess the sensitivity of results.

Specifically, this study aims to:

- Develop a two-stage stochastic programming model to optimize the sizing and annual operation of an HRES while considering multiple uncertainty scenarios with the objective of minimizing Total Annualized Costs (TACs) and CO2 emissions.
- Analyze the effects of variability in renewable energy generation on system sizing and operation, particularly in relation to CO2 emission constraints.
- Ensure system reliability by designing a configuration able to meet the electricity demand under all possible operating conditions.
- Apply the proposed methodology to a real-world case study on Pantelleria, a remote Mediterranean island whose current electricity production is based on diesel generators.

The remainder of the paper is organized as follows: Section 2 describes the modelling approach, optimization framework, and reference case study. Section 3 discusses the main results. Finally, conclusions are provided in Section 4.

## 2. Materials and methods

This study developed an optimization framework to determine the optimal sizing and operation of an off-grid HRES under uncertainty. The framework was based on Linear Programming and developed in Python. Although LP models provide a simplified representation of the system, they are widely employed in stochastic programming [25] In this context, computational complexity grows with the number of scenarios considered, particularly when performing annual simulations at an hourly resolution, as in the present study. The primary limitations of using an LP are the inability to capture the nonlinear efficiency characteristics of energy technologies and to include operational constraints such as minimum load requirements. These limitations are relevant for hydrogen-based technologies, whose performance is significantly affected by partial-load operation. However, the drawback is mitigated by the modular nature of the system, which allows components to operate near their nominal capacity by dynamically adjusting the number of active modules. Additionally, another simplification of LP models compared to MILP is the loss of information regarding non-simultaneity between charging and discharging processes in storage systems. This behavior is automatically managed by the optimization process. Since all components have an efficiency lower than 100 %, energy losses discourage simultaneous charging and discharging, leading the optimizer to separate these operations at each timestep [26].

The optimization process followed a multi-objective approach, implemented through the ε-constraint method [27], which enabled the simultaneous minimization of Total Annualized Costs and CO2 emissions. To account for uncertainties in RES generation, the study integrated a two-stage stochastic optimization framework. The approach ensured that the system is sized to reliably meet demand under all scenarios, preventing power shortages.

To enhance computational feasibility while preserving the statistical characteristics of the uncertainties, a K-means clustering technique [28] was employed for scenario reduction. K-means is capable of efficiently selecting a representative subset of scenarios that are used to characterize the uncertainty.

## 2.1. Energy system modelling

The energy system was modeled as an LP problem, formulated over a one-year time horizon (T) with an hourly resolution. Table 1 presents the nominal operating conditions of the energy system components, while the following sub-sections delve into the modeling details of each component.

**Table 1**
Technical parameters and operating conditions of HRES components.

| Component | Parameter | Units | Value | Ref |
|---|---|---|---|---|
| PV | Tilt | ° | 32 | – |
| | Azimuth | ° | 7 | – |
| | Losses | % | 14 | [29] |
| | Specific production, $\varsigma_{PV}$ | $kWh/kW_p$ | Time series | [29] |
| | Lifetime | years | Project (20) | – |
| Wind | Turbine height, $h_{WT}$ | m | 80 | – |
| | Reference height, $h_{ref}$ | m | 10 | – |
| | Exponent law coefficient, $\alpha$ | [−] | 0.17 | [30] |
| | Cut-in wind speed, $v_{w,ci}$ | m/s | 3 | [31] |
| | Cut-out wind speed, $v_{w,co}$ | m/s | 25 | [31] |
| | Rated wind speed, $v_{w,r}$ | m/s | 13 | [31] |
| | Lifetime | years | Project (20) | – |
| BESS | Charging efficiency, $\eta_{BT,ch}$ | % | 95 | [32] |
| | Discharging efficiency, $\eta_{BT,dis}$ | % | 95 | [32] |
| | C-rate, *Crate* | [−] | 0.9 | [33] |
| | Self-discharge rate, $\sigma$ | [−] | 5 %/month | [34] |
| | Minimum SOC, $SOC_{min}$ | [−] | 0.2 | [34] |
| | Maximum SOC, $SOC_{max}$ | [−] | 1 | – |
| | Lifetime | years | 15 | [35] |
| PEMEL | Operating pressure | bar | 30 | – |
| | Conversion efficiency, $\varepsilon_{EL}$ | $kWh/kg_{H2}$ | 50.5 | [36] |
| | Water Consumption, $\delta_{H2O}$ | $m^3_{H2O}/kg_{H2}$ | 0.015 | [37] |
| | Lifetime | years | 10 | [38] |
| PEMFC | Operating pressure | bar | 1 | – |
| | Nominal efficiency, $\zeta_{FC}$ | $kg_{H2}/kWh$ | 0.060 | [39] |
| | Lifetime | years | 10 | [40] |
| $H_2$ Tank | Nominal pressure | bar | 200 | – |
| | Lifetime | years | Project (20) | – |
| Compressor | Input pressure | bar | 30 | – |
| | Output pressure | bar | 220 | – |
| | Specific consumption, $\varepsilon_{CO}$ | $kWh/kg_{H2}$ | 1.76 | [41] |
| | Lifetime | years | Project (20) | – |
| Diesel Generator | Nominal Efficiency, $\eta_{DG}$ | % | 37 | [39] |
| | $CO_2$ emissions | $kg/m^3$ | 3000 | [42] |
| | Lifetime | years | Project (20) | – |

The proposed HRES configuration is illustrated in Fig. 1, with power generation from WT, PV panels, and DGs, both a BESS and an HSS for power balancing, and an electricity demand of the island. Therefore, at each timestep, the energy balance in Equation (1) must be met.

$$\begin{aligned} &P_{PV}(t)+P_{WT}(t)+P_{FC}(t)+P_{BT,dis}(t)+P_{DG}(t)\\ &\quad=P_{DEM}(t)+P_{EL}(t)+P_{CO}(t)+P_{BT,ch}(t)+P_{CURT}(t) \end{aligned} \tag{1}$$

Where $P_{PV}(t)$, $P_{WT}(t)$ and $P_{DG}(t)$ are the power generated respectively by the PV, the wind turbine, and the DGs, $P_{BT,dis}(t)$ and $P_{BT,ch}(t)$ are the discharging and charging power of the battery, $P_{FC}(t)$, $P_{EL}(t)$ and $P_{CO}(t)$ are the fuel cell, the electrolyzer, and the compressor operating power, $P_{DEM}(t)$ is the electricity demand of the system and $P_{CURT}(t)$ is the power curtailment of RES, all expressed in kW.

### 2.1.1. Photovoltaic system

The potential energy production of the PV system was obtained at the chosen location from the Photovoltaic Geographical Information System (PVGIS) [29] database with an hourly resolution. Solar radiation predictions were sourced from the PVGIS-SARAH 2 dataset. The PV system was modeled as a fixed-tilt installation, with the tilt (32°) and azimuth (7°) angles optimized for the specific location. A 14 % system loss was applied, as recommended by PVGIS, to account for all the factors that cause a decrease in power production, such as cables and inverter losses, dirt accumulation, and long-term module degradation. In this way, a specific energy production $\varsigma_{PV}(t)$ was obtained for each timestep and used to calculate the total power output of the system $P_{PV}(t)$ by multiplying it by the nominal power of the plant $P_{PV,r}$, as expressed in Equation (2):

$$P_{PV}(t)=\varsigma_{PV}(t)\cdot P_{PV,r} \tag{2}$$

### 2.1.2. Wind turbine generators

The power output of the WT was determined based on its characteristic power curve, which relates the power generated to the input wind speed. The power output at the timestep $t$ was calculated as described in Equation (3) [43]:

$$P_{WT}(t)=\begin{cases} 0,\ v_w(t)\le v_{w,ci}\\ P_{WT,r}\cdot\dfrac{v_w^3(t)-v_{w,ci}^3}{v_{w,r}^3-v_{w,ci}^3},\ v_{w,ci}\le v_w(t)\le v_{w,r}\\ P_{WT,r},\ v_{w,r}\le v_w(t)\le v_{w,co}\\ 0,\ v_w(t)\ge v_{w,co}\end{cases} \tag{3}$$

Where $v_{w,ci}$, $v_{w,co}$, and $v_{w,r}$ are respectively the cut-in, cut-out, and rated wind speed (in m/s), while $P_{WT,r}$ is the nominal power of the turbine, in kW.

Wind speed data were retrieved from PVGIS, which provides values at a reference height ($h_{ref}$) of 10 m. Therefore, they were corrected to the turbine height ($h_{WT}$) using the power law reported in Equation (4):

$$v_w(t)=v_{w,ref}(t)\cdot\left(\frac{h_{WT}}{h_{ref}}\right)^{\alpha} \tag{4}$$

Where $v_{w,ref}$ is the wind speed measured at the reference height (in m/s), and $\alpha$ is the exponent of the power law, which depends on the surface topology. For this study, a value of 0.17 was selected for $\alpha$, based on the mean wind speed at the turbine and reference height reported by the Italian Wind Atlas [30].

### 2.1.3. Battery energy storage system

Energy storage systems play a critical role in isolated grids, ensuring the coupling of renewable energy generation with electricity demand. In this study, both a battery energy storage system and a hydrogen-based storage system were analyzed. The BESS selected for this study

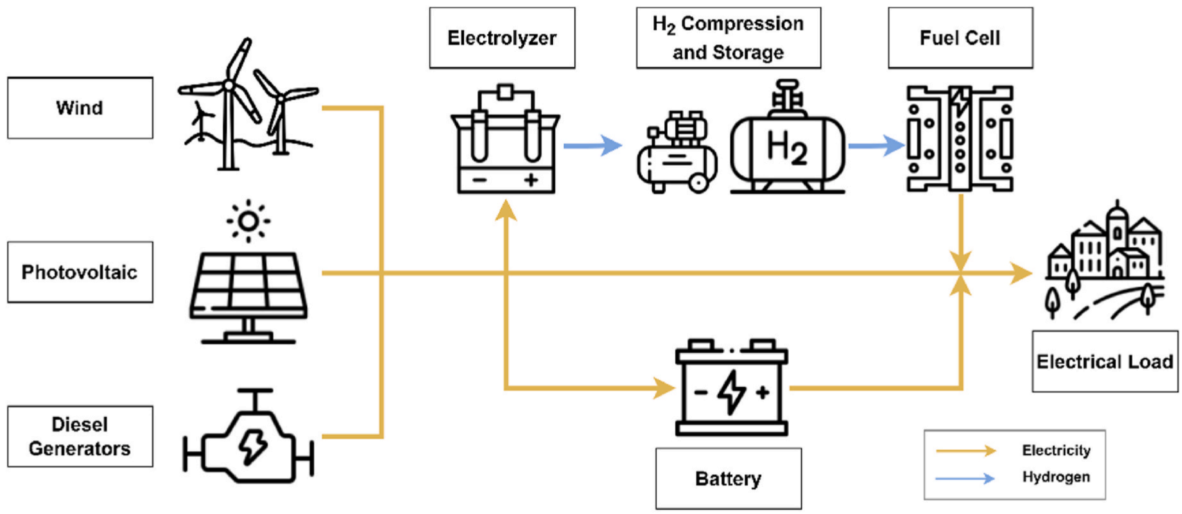


**Fig. 1.** HRES configuration.

employed a lithium-ion technology. Lithium-ion batteries offer higher efficiency, longer lifespan, and improved energy density compared to the lead-acid alternative [44]. The State of Charge (SOC), which represents the ratio of the stored energy to the nominal capacity, was updated dynamically at each timestep following Equation (5):

$$SOC(t+1) = SOC(t)\cdot(1-\sigma) + \frac{P_{BT,ch}(t)\cdot\Delta t\cdot\eta_{BT,ch}}{Cap_{BT}} - \frac{P_{BT,dis}(t)\cdot\Delta t}{Cap_{BT}\cdot\eta_{BT,dis}} \tag{5}$$

Where $\eta_{BT,ch}$ and $\eta_{BT,dis}$ are respectively the BESS charging and discharging efficiencies, $\sigma$ is the hourly self-discharge rate, and $Cap_{BT}$ is the nominal battery capacity (in kWh). To ensure operational safety and prevent deep discharge, the SOC was bounded between a minimum and maximum threshold, as reported in Equation (6). While $SOC_{max}$ was set to 1, a $SOC_{min}$ threshold of 0.2 was imposed for safety reasons [34]:

$$SOC_{min} \leq SOC(t) \leq SOC_{max} \tag{6}$$

Additionally, the SOC at the start and end of the simulation must be consistent to maintain the system energy balance, as reported in Equation (7):

$$SOC(t_{start}) = SOC(t_{end})\cdot(1-\sigma) + \frac{P_{BT,ch}(t_{end})\cdot\Delta t\cdot\eta_{BT,ch}}{Cap_{BT}} - \frac{P_{BT,dis}(t_{end})\cdot\Delta t}{Cap_{BT}\cdot\eta_{BT,dis}} \tag{7}$$

The charge or discharge of the battery at each timestep were managed through Equations (8) and (9):

$$0 \leq P_{BT,ch}(t) \leq Crate\cdot Cap_{BT}/\Delta t \tag{8}$$

$$0 \leq P_{BT,dis}(t) \leq Crate\cdot Cap_{BT}/\Delta t \tag{9}$$

A *Crate* of 0.9 was imposed, meaning that the battery can be charged or discharged up to 90 % of its nominal capacity per hour [33].

### 2.1.4. Hydrogen-based energy storage system

For hydrogen storage, this study considered Proton-Exchange Membrane (PEM) technology for both the electrolyzer (PEMEL) and fuel cell (PEMFC). PEM technology is well-suited for intermittent renewable energy sources due to its fast response time and operational flexibility [45]. The electrolyzer operated at a pressure of 30 bar, with a nominal efficiency of 66.0 %, corresponding to a conversion factor $\varepsilon_{EL}$ of 50.5 kWh/$kg_{H2}$ [36]. The fuel cell functioned at ambient pressure, achieving a nominal efficiency of 50.0 % [39], equivalent to a conversion factor $\zeta_{FC}$ of 0.060 $kg_{H2}$/kWh.

Since renewable energy availability and electricity demand fluctuate, the operating power of the electrolyzer and fuel cell varies dynamically. The LP model did not enforce a minimum power constraint. However, a report by Tractebel and Hinicio [41] indicated that PEM electrolyzers and fuel cells can operate across their entire power range, from zero to their nominal capacity. Despite this, operating at very low partial loads should be discouraged as it accelerates the chemical degradation of the PEM membrane [46].

The Level of Hydrogen (LOH) of the $H_2$ Tank, defined as the ratio of the stored hydrogen to the $H_2$ tank capacity, was dynamically updated at each time step. Coherently with BESS, the LOH constraint must also be met between the first and the last timestep, as shown in Equations (10) and (11):

$$LOH(t+1) = LOH(t) + \frac{m_{H2,EL}(t)\cdot\Delta t}{Size_{HT}} - \frac{m_{H2,FC}(t)\cdot\Delta t}{Size_{HT}} \tag{10}$$

$$LOH(t_{start}) = LOH(t_{end}) + \frac{m_{H2,EL}(t_{end})\cdot\Delta t}{Size_{HT}} - \frac{m_{H2,FC}(t_{end})\cdot\Delta t}{Size_{HT}} \tag{11}$$

Where $m_{H2,EL}$ and $m_{H2,FC}$ are respectively the mass flow of hydrogen produced by the electrolyzer and consumed by the fuel cell at timestep $t$ (in kg/h), and $Size_{HT}$ is the hydrogen tank capacity (in kg). The mass flows were linked to the electrolyzer and fuel cell power via Equations (12) and (13):

$$m_{H2,EL}(t) = P_{EL}(t)/\varepsilon_{EL} \tag{12}$$

$$m_{H2,FC}(t) = P_{FC}(t)\cdot\zeta_{FC} \tag{13}$$

The input power of electrolyzer and fuel cell was limited by Equations (14) and (15):

$$0 \leq P_{EL}(t) \leq P_{EL,r} \tag{14}$$

$$0 \leq P_{FC}(t) \leq P_{FC,r} \tag{15}$$

At any timestep, LOH was constrained between 0 ($LOH_{min}$) and 1 ($LOH_{max}$) as reported in Equation (16):

$$LOH_{min} \leq LOH(t) \leq LOH_{max} \tag{16}$$

The water consumption (in $m^3$/h) for the operation of the PEMEL was computed by multiplying the hydrogen consumption for a water consumption factor $\delta_{H2O}$, equal to 0.015 $m^3_{H20}/kg_{H2}$ [37], as reported in Equation (17):

$$Q_{H2O,EL}(t) = m_{H2,EL}(t)\cdot\delta_{H2O} \tag{17}$$

The hydrogen was stored in a Type 1 seamless steel tank at 200 bar.

Pressure losses due to valves, tubing, and permeation are negligible in these types of tanks [33]. A centrifugal compression system was employed to increase the hydrogen pressure from the PEMEL outlet pressure of 30 bar to the storage pressure. The power consumption of the process was estimated using an adiabatic compression model with an overall efficiency of 50 %, which included both electrical power conversion and auxiliary systems. Further details are in the final report by Tractebel Engie and Hinicio [41]. The outlet pressure of the compressor was 10 % higher [47] than the storage pressure to prevent backflow. The power required by the compressor was calculated as in Equation (18), with the power limited by the nominal power of the compressor as reported in Equation (19):

$$P_{\mathrm{CO}}(t) = m_{\mathrm{H2,EL}}(t) \cdot \varepsilon_{\mathrm{CO}} \tag{18}$$

$$0 \leq P_{\mathrm{CO}}(t) \leq P_{\mathrm{CO,r}} \tag{19}$$

The specific energy consumption $\varepsilon_{\mathrm{CO}}$ for compressing hydrogen was therefore found to be approximately 1.76 $\mathrm{kWh/kg_{H2}}$.

### 2.1.5. Diesel generators

The diesel generators were assumed to operate with load modulation, allowing them to adjust their output to meet the electrical demand dynamically. The power generated by the DGs is bounded between 0 and its nominal power, as in Equation (20):

$$0 \leq P_{\mathrm{DG}}(t) \leq P_{\mathrm{DG,r}} \tag{20}$$

The DGs fuel consumption $Q_{\mathrm{DG}}(t)$ (in $\mathrm{m^3/h}$) was estimated considering its nominal efficiency $\eta_{\mathrm{DG}}$, set to 37 % [39], and the diesel heating value $\mathrm{LHV_{diesel}}$, equal to 10069 $\mathrm{kWh/m^3}$, as reported in Equation (21).

$$Q_{\mathrm{DG}}(t) = P_{\mathrm{DG}}(t) \,/\, (\mathrm{LHV_{diesel}} \cdot \eta_{\mathrm{DG}}) \tag{21}$$

## 2.2. Economic parameters and TAC estimation

The techno-economic data and assumptions used in this study are summarized in Table 2. To ensure the highest level of accuracy, the most up-to-date economic data have been sourced from reliable and authoritative sources, including the International Energy Agency, National Renewable Energy Laboratory (NREL), and Danish Energy Agency (DEA), as well as relevant literature sources.

**Table 2**
Economic parameters.

| Component | $C_{\mathrm{inv}}$ | $C_{\mathrm{O\&M}}$ | Replacement ($\rho$) | Ref |
|---|---|---|---|---|
| PV | 1060 €/kW | 2 % $C_{\mathrm{inv,PV}}$ | – | [51, 52] |
| Wind | 1200 €/kW | 3 % $C_{\mathrm{inv,wind}}$ | – | [53] |
| BESS | 450 €/kWh | 2.5 % $C_{\mathrm{inv,BESS}}$ | 50 % $C_{\mathrm{inv,BESS}}$ | [35, 54] |
| PEMEL | 1196 €/kW | 5 % $C_{\mathrm{inv,PEMEL}}$ | 50 % $C_{\mathrm{inv,PEMEL}}$ | [55] |
| PEMFC | 1300 €/kW | 5 % $C_{\mathrm{inv,PEMFC}}$ | 20 % $C_{\mathrm{inv,PEMFC}}$ | [39] |
| $H_2$ Tank | 230 €/kg | 2 % $C_{\mathrm{inv,HT}}$ | – | [56] |
| Compressor | 4577 €/kW | 4 % $C_{\mathrm{inv,CO}}$ | – | [57] |
| Diesel Generator | 343 €/kW | 2.5 % $C_{\mathrm{inv,DG}}$ | – | [39] |
| **Energy costs** | **Symbol** | **Value** | | **Ref** |
| Diesel specific cost | $sc_{\mathrm{diesel}}$ | 1800 €/$\mathrm{m^3}$ | | [58] |
| Water specific cost | $sc_{\mathrm{H2O}}$ | 4 €/$\mathrm{m^3}$ | | [59] |
| **Financial parameters** | **Symbol** | **Value** | | **Ref** |
| Nominal discount rate | $dr'$ | 7 % | | [49] |
| Inflation rate | $ir$ | 2.23 % | | [50] |
| Engineering cost | $c_{\mathrm{eng}}$ | 15 % $C_{\mathrm{inv}}$ | | – |
| Installation cost | $c_{\mathrm{inst}}$ | 15 % $C_{\mathrm{inv}}$ | | – |
| Personnel cost | $C_{\mathrm{pers}}$ | 200 k€ | | – |
| Project lifetime | $n_y$ | 20 years | | – |

The economic parameter chosen for the optimization was the Total Annualized Costs, which can be defined as the sum of all capital and operational expenditures of the energy system, expressed as an equivalent annual cost over its lifetime. It accounts for the initial investment, periodic component replacements, and recurring operational expenses. The formula for estimating the Total Annualized Costs (in €) is presented in Equation (22):

$$TAC = CAPEX + OPEX \tag{22}$$

Where *CAPEX* (in €) represents the Capital Expenditures and *OPEX* (in €) represents the Operating Expenditures. *CAPEX* term is composed of the investment ($C_{\mathrm{inv}}$) and replacement cost of each component, with additional engineering ($c_{\mathrm{eng}}$) and installation ($c_{\mathrm{inst}}$) costs as a percentage of the investment, as expressed in Equation (23):

$$CAPEX = \sum_i \left( C_{\mathrm{inv},i} \cdot A_i \cdot (1 + R_i \cdot \rho_i) \right) \tag{23}$$

Where $R_i$ is the number of replacements during the component lifetime, $\rho_i$ is the replacement rate , $A_i$ is the annuity factor of each component, and $i$ is the index referred to the i-th component of the system. The annuity factor is calculated as in Equation (24):

$$A_i = \frac{dr(1+dr)^{lt_i}}{(1+dr)^{lt_i} - 1} \tag{24}$$

Where $lt_i$ is the lifetime of the component, reported in Table 1, and $dr$ is the real discount rate, which takes into account the nominal discount rate ($dr'$) and the inflation rate ($ir$) through Fisher equation [48], as displayed in Equation (25). The nominal discount rate was set at 7 % [49], while the inflation rate was based on the last 30-years average in the Euro Area, set to 2.23 % [50].

$$dr = \frac{1 + dr'}{1 + ir} - 1 \tag{25}$$

The term *OPEX* is instead calculated as in Equation (26):

$$OPEX = \sum_i C_{\mathrm{O\&M},i} + \sum_{t=1}^{T} \left( sc_{\mathrm{H2O}} \cdot Q_{\mathrm{H2O,EL}}(t) \cdot \Delta t + sc_{\mathrm{diesel}} \cdot Q_{\mathrm{DG}}(t) \cdot \Delta t \right) + C_{\mathrm{pers}} \tag{26}$$

Where $C_{\mathrm{O\&M},i}$ is the operation and maintenance cost of the i-th component, expressed as a percentage of its capital cost, the cost of water for the PEMEL and of diesel for the DG calculated are calculated by multiplying the specific cost of demineralized water ($sc_{\mathrm{H2O}}$) and of diesel ($sc_{\mathrm{diesel}}$) (in €/$\mathrm{m^3}$) respectively for the water consumption ($Q_{\mathrm{H20,EL}}$) and diesel consumption ($Q_{\mathrm{DG}}$), and $C_{\mathrm{pers}}$ represents the personnel cost which was assumed equivalent to 200 k€/year for a 24 h supervision of the system (three operators with 8 h shifts).

## 2.3. Sizing approach

### 2.3.1. Multi-objective optimization

The sizing and operation of the system were formulated by solving an LP problem. The model simultaneously determined the optimal system sizing and the hourly dispatch strategy, ensuring that electricity demand is met throughout the year.

It incorporated:

- Hourly time series data for electricity demand and meteorological conditions.
- Technical and economic parameters of each system component.
- Uncertainty modeling, considering multiple scenarios of renewable generation and sensitivity analysis to electricity demand.

The decision variables included:

- Component sizes, which were optimized within predefined bounds.
- Operational variables, such as the input/output power of the electrolyzer and fuel cell, the charging/discharging of the battery, and the power produced by the diesel generator for each timestep, and state variables, as the energy stored in the hydrogen tank and in the battery, and the curtailed renewable energy at each timestep.

The objective was to design the system to minimize the TACs and the $CO_2$ emissions. The multi-objective optimization was performed using the ε-constraint method [27]. The ε-constraint method is a technique that transforms a multi-objective problem into a series of single-objective ones by optimizing one objective while treating the other as a constraint. This method allows the exploration of the trade-off between the two objectives and the construction of the Pareto front. In this study, optimization minimizes TACs while $CO_2$ emissions are imposed as an upper-limit constraint. In particular, a single-objective optimization was initially conducted without imposing any constraint on the emissions, whereas the objective function was to minimize TACs while ensuring that all technical and energy balance constraints were satisfied. The $CO_2$ emissions corresponding to the cost-optimal configuration were then calculated as in Equation (27):

$$m_{CO_2} = \sum_{t=t_{start}}^{t_{end}} Q_{DG}(t) \cdot \Delta t \cdot em_{CO_2,DG} \tag{27}$$

Where $em_{CO_2,DG}$ (in kg/m$^3$) is the $CO_2$ emissions coefficient for diesel fuel, equal to 3000 kg/m$^3$ [42].

To construct the Pareto front, the range between maximum emissions ($m_{CO_2,max}$) and minimum emissions ($m_{CO_2,min}$) was divided into several discrete steps. The minimum emissions were set to zero to represent a fully renewable energy system. A series of single-objective optimizations were then performed, each minimizing TACs while subject to a progressively stricter $CO_2$ emission constraint ($m_{CO_2,target}$), as reported in Equation (28):

$$m_{CO_2} \le m_{CO_2,target} \tag{28}$$

Each single optimization problem can therefore be summarized by Equation (29), where TACs are minimized and emissions explicitly appear as an inequality constraint, consistent with the ε-constraint approach.

$$\begin{aligned} \min \quad & TAC \\ \text{s.t.} \quad & \text{Equality constraints} \quad (1)-(3),(5),(7),(10)-(13),(17),(18),(21) \\ & \text{Inequality constraints} \quad (6),(8),(9),(14)-(16),(19),(20),(28) \end{aligned} \tag{29}$$

### 2.3.2. Two-stage stochastic optimization

When considering an off-grid HRES, parameters such as energy produced by RES or end-user demand have a certain degree of uncertainty. In this study, a two-stage stochastic programming was employed to evaluate the impact of RES production uncertainty on component sizing. In stochastic programming, optimization problems that involve uncertainty are modeled by generating a finite number of scenarios, which correspond to a probability of occurrence. In two-stage stochastic programming, decision variables are divided into two groups:

- First-stage variables: represent the component sizes, which must remain identical across all scenarios to ensure a single system design.

**Table 3**
Energy system variables.

| Component | First-stage Variables | Symbol | Second-stage Variables | Symbol |
|---|---|---|---|---|
| PV | Nominal PV power | $P_{PV,r}$ | PV power production | $P_{PV}(t,s)$ |
| WT | Nominal WT power | $P_{WT,r}$ | WT power production | $P_{WT}(t,s)$ |
| BESS | Nominal BESS capacity | $Cap_{BT}$ | BESS charge power<br>BESS discharge power<br>BESS state of charge | $P_{BT,ch}(t,s)$<br>$P_{BT,dis}(t,s)$<br>$SOC(t,s)$ |
| $H_2$ Tank | Nominal $H_2$ Tank capacity | $Size_{HT}$ | $H_2$ Tank level of hydrogen | $LOH(t,s)$ |
| PEMEL | Nominal PEMEL power | $P_{EL,r}$ | PEMEL power consumption<br>PEMEL hydrogen production<br>PEMEL water consumption | $P_{EL}(t,s)$<br>$m_{H2,EL}(t,s)$<br>$Q_{H2O,EL}(t,s)$ |
| PEMFC | Nominal PEMFC power | $P_{FC,r}$ | PEMFC power production<br>PEMFC hydrogen consumption | $P_{FC}(t,s)$<br>$m_{H2,FC}(t,s)$ |
| Compressor | Nominal Compressor power | $P_{CO,r}$ | Compressor power consumption | $P_{CO}(t,s)$ |
| DG | Nominal DG power | $P_{DG,r}$ | DG power production<br>DG diesel consumption | $P_{DG}(t,s)$<br>$Q_{DG}(t,s)$ |
| Demand | – | – | Electricity demand | $P_{DEM}(t,s)$ |
| Curtailment | – | – | Power curtailment | $P_{CURT}(t,s)$ |

- Second-stage variables: include operational decisions, which are adjusted dynamically in response to each scenario's variability and are therefore dependent on the timestep and the scenario.

All the variables regarding the energy system are reported in Table 3.

In particular, it is essential to ensure that the constraints related to energy balances of the system, technical parameters of the components, and $CO_2$ emissions are satisfied not only for each timestep, but also for each scenario. In this context, the objective function became the sum of the Total Annualized Costs across all scenarios weighted on the probability of the corresponding scenario. Given the uniformity of the component sizes and, consequently, of the components' O&Ms, (first-stage variables), the objective function's variability across scenarios was determined directly by the parameters of water consumption in the electrolyzer and diesel consumption in the diesel generator, as reported in Equations (30) and (31):

$$\overline{TAC} = CAPEX + \overline{OPEX} \tag{30}$$

$$\overline{OPEX} = \sum_i C_{O\&M,i} + C_{pers} + \sum_{s=1}^{S} \left( \sum_{t=1}^{T} \left( sp_{,H2O} \cdot Q_{H2O,EL}(s,t) \cdot \Delta t + sp_{diesel} \cdot Q_{DG}(s,t) \cdot \Delta t \right) \right) \cdot p(s) \tag{31}$$

Where $S$ is the number of scenarios and $p(s)$ is the probability of each scenario $s$. The probability of each scenario was calculated as the outer product of the probability of PV scenarios and wind scenarios, as shown in Equation (32):

$$p(s) = p_{PV}(s_{PV}) \otimes p_{WT}(s_{WT}) \tag{32}$$

This formulation ensures that the system is sized considering all analyzed scenarios. The logical diagram in Fig. 2 elucidates the details of

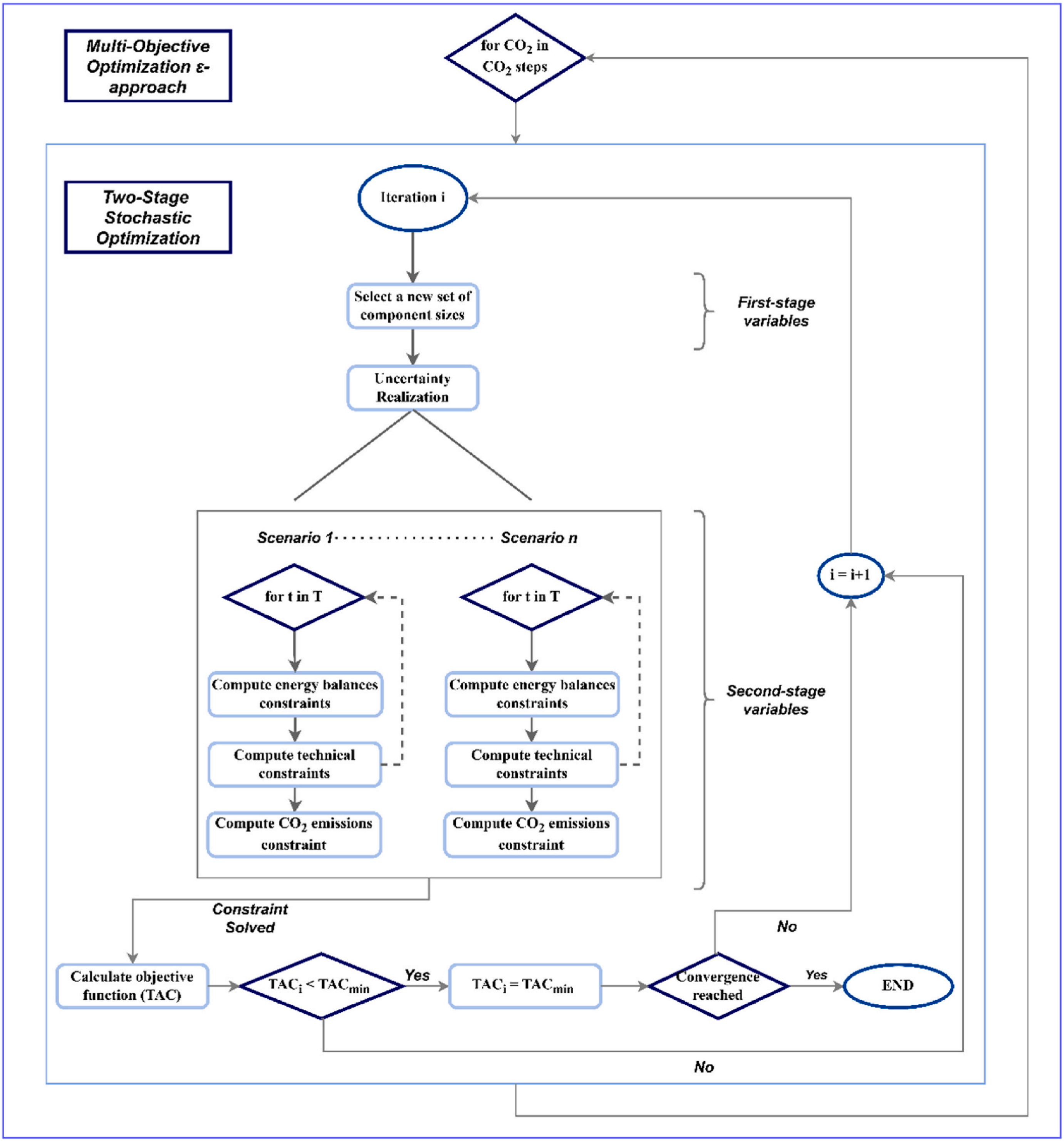


**Fig. 2.** Logical block of the Two-Stage Stochastic Optimization.

the two-stage stochastic multi-objective optimization process.

### 2.4. Pantelleria case study

The island of Pantelleria was selected as a case study for this analysis due to its geographical isolation and renewable energy potential. Given its considerable distance from the mainland, connecting the island to the national electricity grid would be economically unfeasible. Furthermore, Pantelleria currently relies predominantly on diesel generators for electricity generation, which is incompatible with global decarbonization goals. However, the island possesses a high potential for RES, which could facilitate the transition.

A comprehensive analysis of historical RES productivity data from 2005 to 2023 was conducted, covering both photovoltaic and wind energy. The analysis indicated that the mean annual energy yield from PV amounted to 1619 kWh/kW$_p$, corresponding to a capacity factor of 18.5 %, while the mean annual energy yield from wind energy was 3495 kWh/kW$_p$, corresponding to a capacity factor of 39.9 %. Both energy sources are characterized by not negligible variability.

To characterize uncertainty, the full dataset of historical producibility was analyzed as explained in Section 2.5. For the deterministic analysis, it was reasonable to hypothesize that the utilization of the hourly average of historical data would be the optimal approach. While this methodology may be considered valid for solar energy, which follows a well-defined daily pattern, it is less suitable for wind energy. Unlike solar radiation, wind productivity exhibits irregular hourly patterns. This issue is illustrated in Fig. 3, which presents the violin plot of historical wind and solar energy production data for the months of January and July, highlighting the mean values with dark points. Two main considerations can be derived:

- Solar energy is higher in summer, while wind energy has higher productivity in winter.
- Solar energy has a clear daily profile, while wind power output is highly concentrated at extreme values, meaning that the mean value does not accurately represent the true distribution of wind energy availability. If an average profile were used for wind, it would result in an artificially smooth curve, leading to unrealistic predictions and misinterpretation of the system performance.

Following the last consideration, a single year was utilized for the deterministic analysis to capture the real variability. In particular, the year 2005 was chosen as reference, as its annual PV and wind energy production are the closest to the long-term mean values, being equal respectively to 1633.7 kWh/$kW_p$ and 3534.7 kWh/$kW_p$. Consequently, this year is the most representative to compare with the stochastic results.

On the other hand, electricity consumption data were reconstructed using monthly real data from the "Clean Energy for EU Islands" report [58]. The hourly demand profile was derived using the Italian agency for energy system research (RSE) tool TOTEM [60] (Territory Overview Tool for Energy Modelling) for the Province of Trapani. The demand profile exhibits a seasonal trend, with higher electricity consumption in summer, driven by tourism-related activities. The total annual electricity demand was estimated at 31.1 GWh. Fig. 4 summarizes the hourly and monthly energy potential and load profiles over a year.

### 2.5. Uncertainty characterization

Accurately characterizing uncertainties is crucial for two-stage stochastic optimization. RES exhibit strong temporal autocorrelation, making the creation of representative long-term scenarios particularly challenging. It is essential to ensure that the generated scenarios capture seasonal variability while maintaining realistic hourly trends in productivity. To address these challenges, this study employed a Monte Carlo-based scenario generation method. Monte Carlo is an effective algorithm for uncertainty modeling that has been extensively applied to generate scenarios of renewable energy power output [61]. The accuracy of this method depends on the large scale of sampled scenarios. To enhance data recombination and improve statistical representativeness, Bootstrap resampling was incorporated, following a methodology similar to that used by Tapetado and Usaola [62].

In the first stage of the scenario generation process, historical hourly data for photovoltaic and wind energy production over multiple years were organized and grouped by month. Within each month, daily profiles (24-h segments) were extracted to preserve the pattern of RES production. Each scenario was created by randomly selecting a set of daily profiles for each month from the historical data set. By preserving the structure of entire daily profiles, this approach ensures that the temporal correlation between consecutive hours within a day is maintained. The full-year scenario was constructed by concatenating the sampled daily profile across all months, as reported in Equation (33):

$$\boldsymbol{X}^s = \bigcup_{m=1}^{12} \bigcup_{d^*=1}^{n_{d,m}} \boldsymbol{x}_{m,d^*} \tag{33}$$

Where $\boldsymbol{X}^s$ is the annual array of synthetic energy output (PV or wind power) in scenario $s$ and $\boldsymbol{x}_{m,d^*}$ is a randomly selected daily profile, where $d^*$ is randomly selected from historical data and $n_{d,m}$ is the number of days in each month.

Unlike methods that rely on hourly-level sampling, which fail to consider the intrinsic temporal correlation, this approach ensures that variability in renewable energy generation is preserved. While more

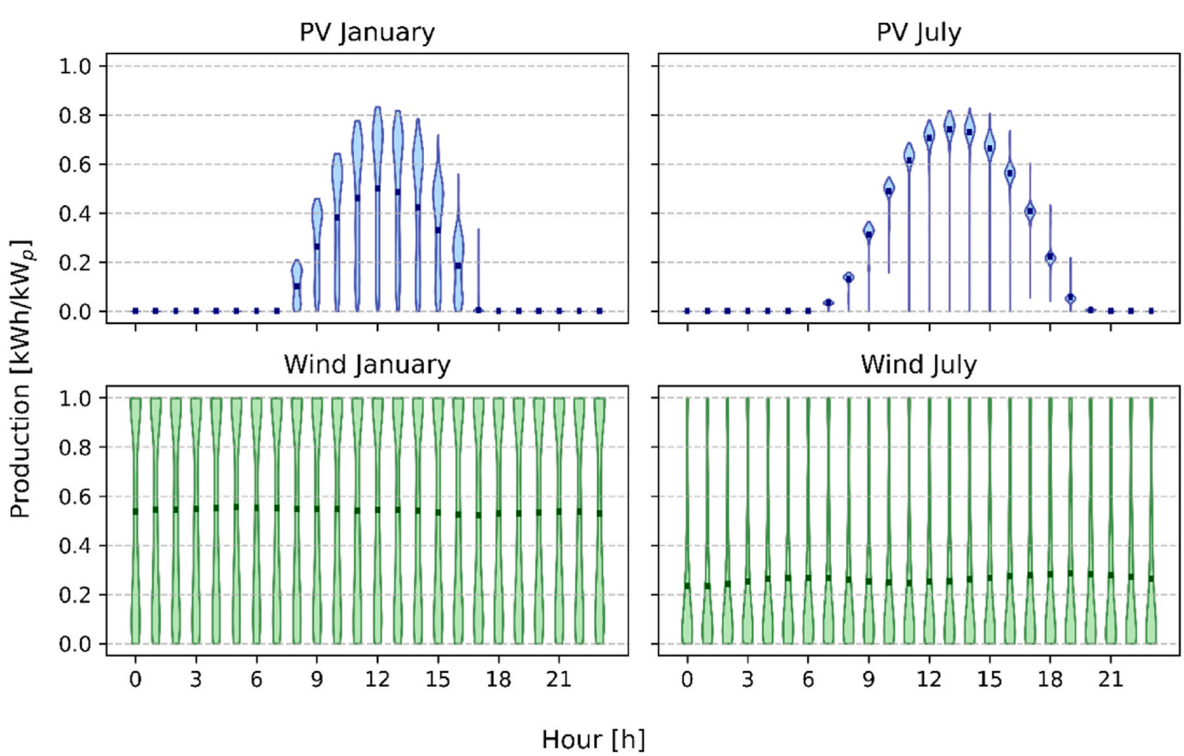


**Fig. 3.** Violin plot of historical data for PV and wind energy producibility in the months of January and July.

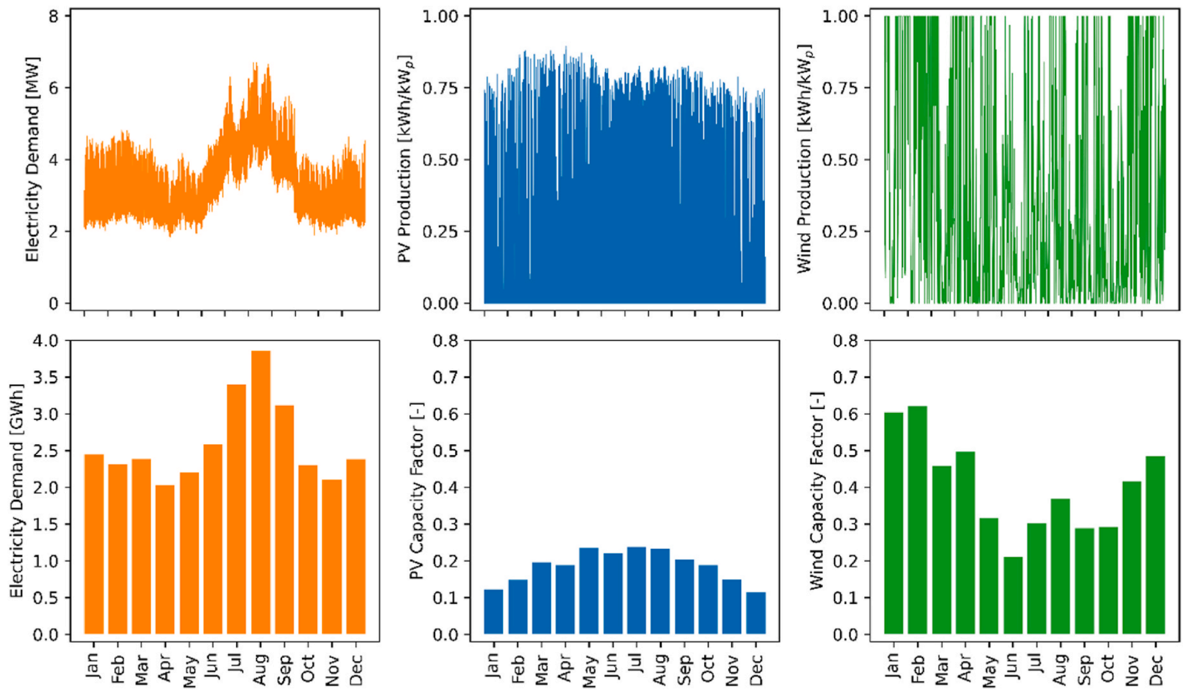


**Fig. 4.** Input renewable energy potential for reference year and load data profile: electrical load, PV energy productivity and wind energy productivity with hourly (top) and monthly (bottom) resolution.

advanced techniques (e.g., autoregressive models or copulas) could be employed, the Monte Carlo-Bootstrap approach offers a computationally efficient alternative that fully exploits the availability of historical data.

To ensure computational feasibility, the initially generated 10000 scenarios were reduced to a manageable number (10) using K-means clustering. This technique identifies k centroids that minimize intra-cluster variance, ensuring that each centroid represents the behavior of its cluster, as shown in Equation (34):

$$\underset{S_{\mathrm{MC}}}{\operatorname{argmin}} \sum_{i=1}^{S_{\mathrm{CL}}} \sum_{s \in S_i} \left\| \sum_{\boldsymbol{x}_{m,d^*} \in \boldsymbol{X}^s} \sum_{x(t) \in \boldsymbol{x}_{m,d^*}} x(t) - \mu^i \right\|^2 \tag{34}$$

Where $S_{\mathrm{MC}}$ is the number of generated scenarios (10000), $S_{\mathrm{CL}}$ is the number of clusters (10), and $\mu^i$ is the centroid of cluster $i$.

The centroids were therefore selected as the reduced set of representative scenarios. To preserve the statistical properties of the original dataset, the probability of each reduced scenario was determined based on the proportion of original scenarios assigned to its corresponding cluster. Fig. 5 presents the histogram of generated scenarios for PV and wind energy, divided by cluster with the scenario reduction technique. The red circles indicate the representative cluster centroids and their associated probabilities. As 10 scenarios were selected for both photovoltaic and wind energy, a total of 100 scenarios were utilized for stochastic optimization. Table 4 summarizes the values of the representative scenarios, along with their deviation from the weighted mean. A higher variability was detected in annual wind energy production, consistent with historical data and previous findings in the literature [63].

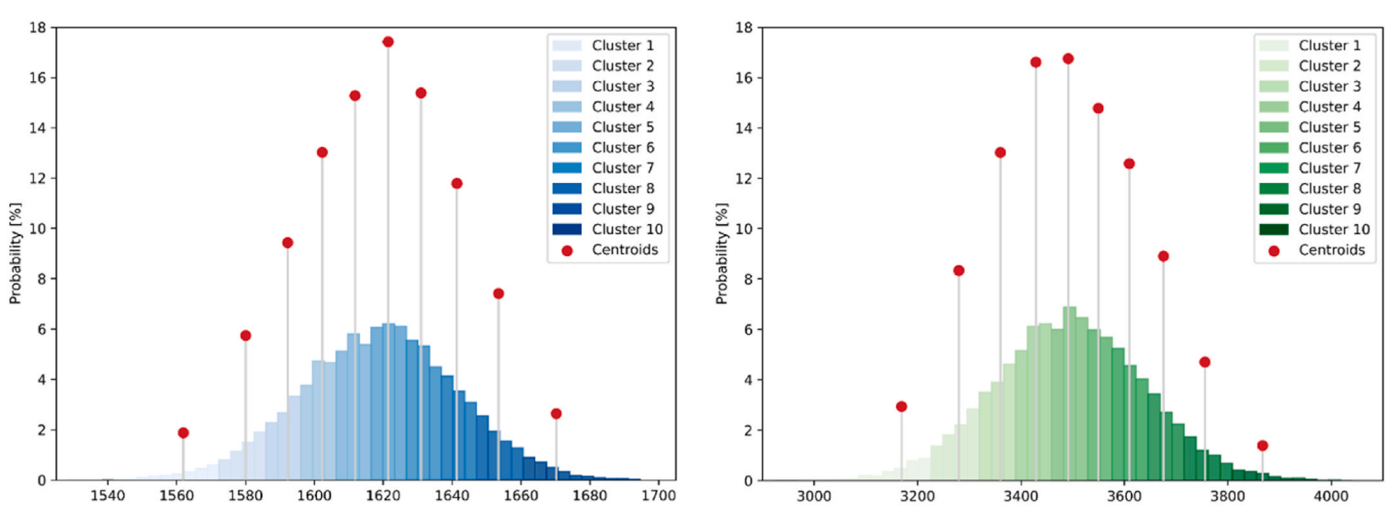


**Fig. 5.** Histogram of PV and wind scenario generation, clustering and reduction.

**Table 4**
Specific Production, probability and distance from weighted mean of selected scenarios for PV and wind.

| RES | Scenario | Specific Production [kWh/kW$_p$] | Probability [%] | Weighted Mean [kWh/kW$_p$] | Distance from Weighted Mean [%] |
|---|---|---|---|---|---|
| PV | 1 | 1562.0 | 1.88 | 1618.7 | −3.50 |
| | 2 | 1580.1 | 5.74 | | −2.38 |
| | 3 | 1592.2 | 9.43 | | −1.64 |
| | 4 | 1602.3 | 13.02 | | −1.01 |
| | 5 | 1611.8 | 15.28 | | −0.43 |
| | 6 | 1621.4 | 17.42 | | 0.17 |
| | 7 | 1631.0 | 15.39 | | 0.76 |
| | 8 | 1641.4 | 11.74 | | 1.40 |
| | 9 | 1653.4 | 7.41 | | 2.14 |
| | 10 | 1670.2 | 2.64 | | 3.18 |
| Wind | 1 | 3169.0 | 2.94 | 3494.2 | −9.31 |
| | 2 | 3279.8 | 8.33 | | −6.14 |
| | 3 | 3359.9 | 13.02 | | −3.84 |
| | 4 | 3428.7 | 16.61 | | −1.87 |
| | 5 | 3491.3 | 16.75 | | −0.08 |
| | 6 | 3549.5 | 14.78 | | 1.58 |
| | 7 | 3609.5 | 12.58 | | 3.30 |
| | 8 | 3675.7 | 8.90 | | 5.19 |
| | 9 | 3755.6 | 4.70 | | 7.48 |
| | 10 | 3867.2 | 1.39 | | 10.67 |

## 3. Results and discussion

### 3.1. Deterministic optimization results

The electricity demand of the island of Pantelleria is currently supplied by 22 MW of DGs, complemented with a 1 MW PV system [58]. In this configuration, PV covers only 5.2 % of the electricity demand, while the remaining 94.8 % is met by DGs. The quantity of diesel required amounts to 7900 m$^3$. Diesel purchase represents the primary cost component, leading to Total Annualized Costs of approximately 15.5 M€, with associated $CO_2$ emissions of 23.7 kt/y. This quantity of $CO_2$ corresponds to an emission factor of 762 $g_{CO2}$/kWh, which is more than 3 times higher than the Italian electricity grid value of 2024 (274 $g_{CO2}$/kWh [64]).

As previously described, the multi-objective optimization was performed using the ε-constraint method, where the minimization of TACs is the objective function and $CO_2$ emissions are progressively reduced. The analysis identified the lowest cost-scenario – with TACs of 6.38 M€ - at an emission level of 3.2 kt/y (103 $g_{CO2}$/kWh). This outcome already highlights the potential for significant emission reductions while considerably improving economic performance. Following the identification of this cost-optimal configuration, the optimization was extended by progressively imposing stricter $CO_2$ emissions constraints, with incremental steps of 0.4 kt/y. Additionally, two emission values of 0.1 and 0.25 kt/y were introduced to better characterize the transition toward a zero-emission system. The resulting Pareto front, illustrated in Fig. 6, compares the optimized configurations with the current energy mix, with pie charts representing electric load coverage in three key cases:

- Current scenario
- Minimum-cost scenario
- Zero-emissions scenario (100 % RES-based system).

A detailed analysis of the Pareto Front reveals that all optimized scenarios yield substantial reductions in both TACs (−47.7 % to −58.8 %) and emissions (−100 % to −86.5 %). The lowest-cost configuration achieves TACs of 6.38 M€, with a load coverage distribution of 12.5 % from DGs, 66.2 % directly from RES, 15.1 % from battery, and 6.2 % from the hydrogen system. In the zero-emissions scenario, costs increase by 27.0 % (8.10 M€) compared to the most cost-efficient case. Here, 65.8 % of the electricity demand is directly met by RES, 24.9 % from BESS, and 9.3 % from HSS. The predominance of demand coverage by the battery over the fuel cell can be observed in both cases. This predominance is attributed to the fact that batteries primarily handle short-term energy balancing, while the hydrogen system is utilized for medium-to-long term storage. Additionally, a sharp cost increase is observed in the final $CO_2$ emissions reduction steps, emphasizing the complexity and challenges associated with transitioning to a fully renewable energy system, where the flexibility provided by diesel generators is lost.

The minimum TACs configuration is achieved with the following

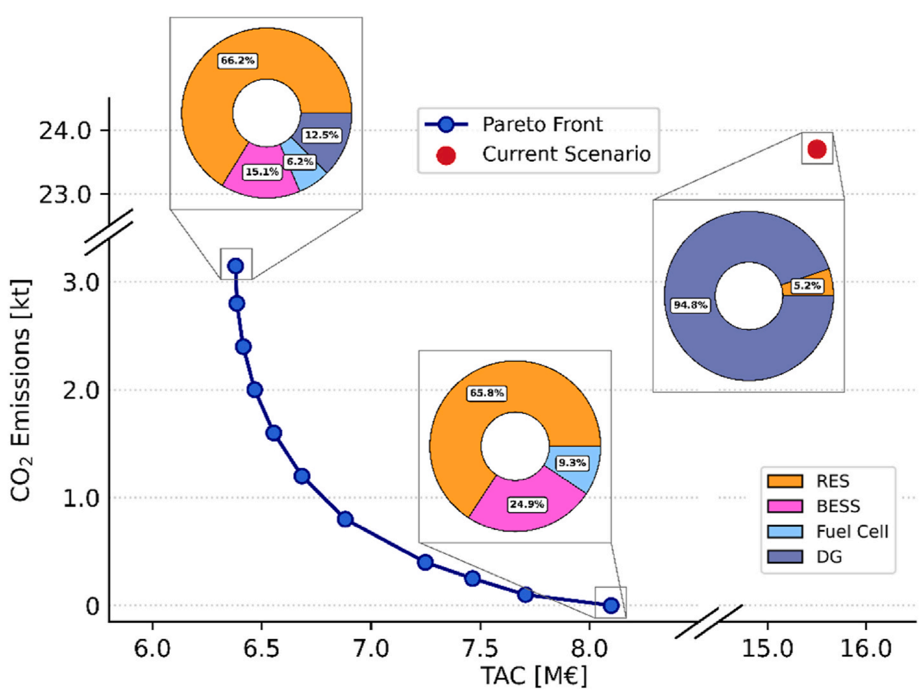


**Fig. 6.** Cost-emission Pareto Front for deterministic scenario compared with reference case with pie charts of electricity demand coverage.

component sizes: approximately 9.7 MW of PV, 8.8 MW of WT, 3.3 MW of DG, 11.2 MWh of BESS, 1.6 MW of PEMEL, 1.0 MW of PEMFC, and 4.2 t (139 MWh) of $H_2$ tank. Fig. 7 illustrates how optimal component sizes evolve as $CO_2$ emissions constraint becomes more stringent. In general, a stricter emission constraint leads to an increase in PV and WT capacities, a reduction in DG size, and an expansion of storage systems. In particular, in the zero-emissions scenario, PV and WT power rise to 15.8 MW (+62.9 %) and 10.8 MW (+22.7 %), respectively, while diesel generators are not employed. Consequently, the fully renewable system necessitates a substantial increase in storage capacity, as DGs can no longer compensate for the intermittency of renewable energy sources. The BESS capacity grows to 24.6 MWh (+119.6 %), while the hydrogen system shows the most significant size expansion, with the PEMEL reaching 3.4 MW (+116.6 %), the PEMFC increasing to 3.5 MW (+253.5 %) and the $H_2$ tank capacity growing to 28.1 t (936 MWh) (+564.3 %). Notably, the fuel cell and hydrogen tank sizes experience a steep increase in scenarios with very stringent $CO_2$ emissions constraints.

From an economic point of view, the increase in renewable generation and storage capacities – driven by stricter $CO_2$ emissions constraints – leads to higher system costs, as evidenced by the Pareto front in Fig. 6. Fig. 8 provides a detailed breakdown of components contribution to TACs. As diesel consumption decreases, the cost contribution of DGs is concurrently reduced, while the contribution of other components is increased. In particular, DG-related costs decrease from 2.00 M€ in the minimum TACs scenario to zero where no emissions are allowed. On the other hand, PV and WT costs range from 1.00 M€ to 1.64 M€ and from 1.14 M€ to 1.39 M€, respectively. Similarly, the contributions of battery and hydrogen storage systems rise from 0.60 M€ to 1.32 M€ and from 0.69 M€ to 2.23 M€. Additionally, as system size grows, the costs associated with engineering and installation also increase (while personnel costs are constant), ranging from 0.93 M€ to 1.52 M€.

Table 5 presents a comprehensive overview of these costs in the two extreme configurations (minimum TACs and zero-emissions), along with the percentage impact on total costs of each component. The table also provides a detailed breakdown of the costs of individual components of HSS.

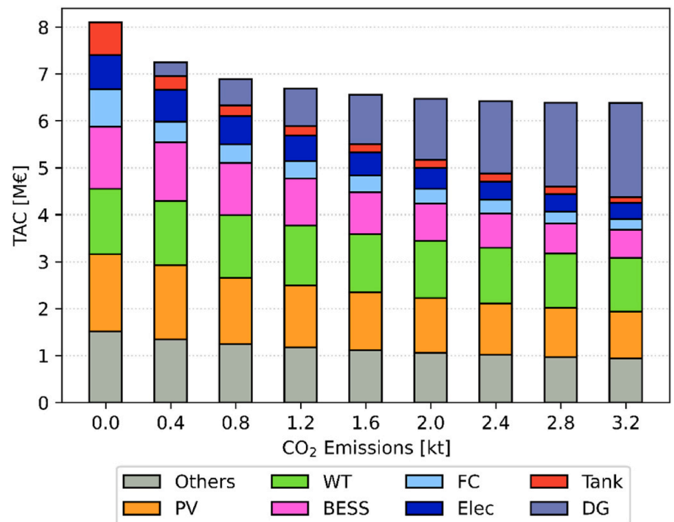


**Fig. 8.** TACs variation with $CO_2$ emissions constraint. "Others" include engineering, installation and personnel. Component costs include CAPEX and OPEX. Compressor is included in Tank costs.

**Table 5**
Contribution on TACs of components for zero emissions and minimum TACs scenarios.

| Scenario | Zero-Emissions | | Minimum TACs | |
|---|---|---|---|---|
| Component | Cost [M€] | Impact on TACs [%] | Cost [M€] | Impact on TACs [%] |
| PV | 1.64 | 20.24 | 1.00 | 15.67 |
| WT | 1.39 | 17.16 | 1.14 | 17.87 |
| BESS | 1.32 | 16.30 | 0.60 | 9.40 |
| FC | 0.80 | 9.88 | 0.23 | 3.61 |
| Elec | 0.73 | 9.01 | 0.34 | 5.33 |
| Tank | 0.70 | 8.64 | 0.13 | 2.04 |
| DG | – | – | 2.01 | 31.50 |
| Others | 1.52 | 18.77 | 0.93 | 14.58 |
| Total | 8.10 | 100 | 6.38 | 100 |

### 3.2. Stochastic optimization results

The stochastic approach significantly impacts the Pareto front, as illustrated in Fig. 9. In the deterministic case, each optimization run corresponds to a single set of input parameters, while the stochastic Pareto front is obtained by solving multiple scenarios simultaneously. This approach, driven by the uncertainty in renewable energy generation, ensures that system sizing satisfies all the constraints, including the one about $CO_2$ emissions, across all scenarios. As a result, the stochastic Pareto front is fan-shaped, and the mean stochastic curve for a given ε-constraint exhibits lower average emissions compared to the deterministic counterpart. For scenarios with high allowable emissions, diesel generators act as a buffer, maintaining average costs comparable to the deterministic case. However, this comes at the expense of increased uncertainty due to the variability in diesel consumption (and with lower economic impact on water consumption). Conversely, at low emissions levels, the flexibility provided by DGs is lost, necessitating larger system components to ensure demand coverage in all the scenarios, ultimately leading to higher costs. In particular, in the zero-emissions scenario, system costs increase by 15.7 %, rising from 8.10

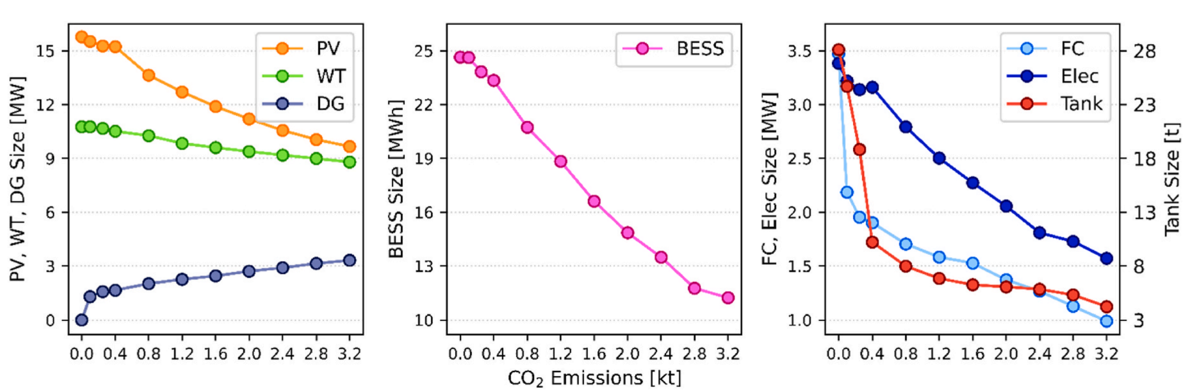


**Fig. 7.** Component sizes variation with $CO_2$ emissions constraint.

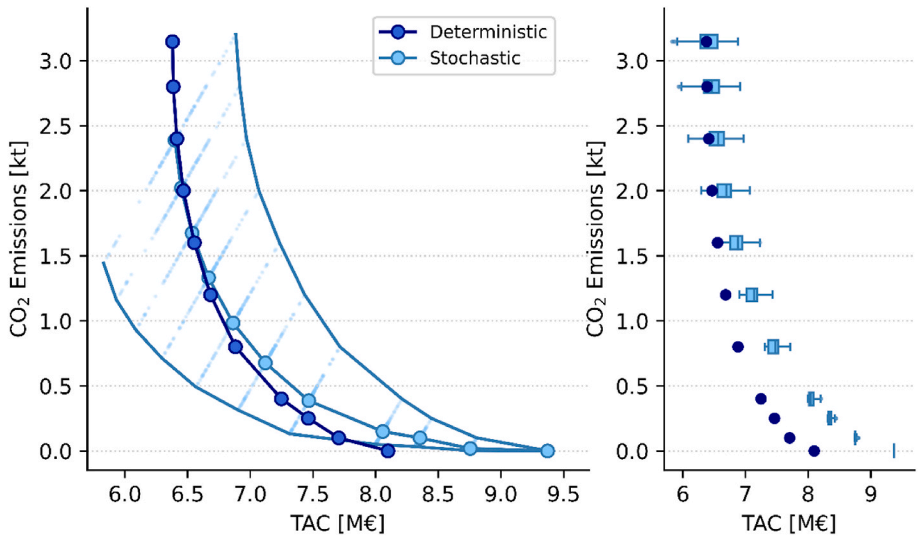


**Fig. 9.** Cost-emissions Pareto Front in deterministic and in stochastic scenarios, with min-max range (left) and comparison of costs at the same emissions level with boxplot for stochastic scenario (right).

M€ to 9.37 M€. Table 6 provides an overview of the impact of RES generation uncertainty on TACs.

Fig. 10 shows the required increase in component sizes in the stochastic zero-emissions scenario compared to the deterministic one. The photovoltaic system size increases from 15.8 MW to 18.6 MW, while the wind turbine power exhibits a modest decrease from 10.8 MW to 10.3 MW. However, the most significant changes occur in storage systems: the battery storage capacity expands from 24.6 MWh to 38.8 MWh (+59.0 %), and the hydrogen storage tank increases from 28.1 t to 34.6 t (+23.1 %). Thus, while stochastic optimization ensures a more resilient system design, it also results in a more expensive configuration as the components are conservatively sized considering all possible scenarios.

The absence of diesel generators in the zero-emissions configuration has the further consequence of higher variability in the utilization of storage systems across different scenarios. This variability is necessary to compensate for the differences in RES generation scenarios. This necessity is particularly evident in hydrogen storage, as highlighted in Fig. 11, which illustrates the evolution of the LOH over the year. The stochastic results exhibit significant variability, with the Interquartile Range (IQR) and minimum-maximum bounds demonstrating the wide range of possible hydrogen levels depending on the scenario. In scenarios with high renewable generation, exemplified by the dashed green line, the system experiences a smaller delta between the minimum and maximum hydrogen levels, indicating that a smaller storage capacity would have been sufficient. On the other hand, scenarios with lower RES production, represented by the dashed red line, require higher fuel cell utilization and, consequently, higher hydrogen storage size. Appendix A

**Table 6**
Stochastic optimization impact on system TACs at different $CO_2$ emissions levels.

| Scenario | Deterministic | Stochastic | | | |
|---|---|---|---|---|---|
| $CO_2$ Emissions [kt] | TAC [M€] | Mean TAC [M€] | Min TAC [M€] | Max TAC [M€] | Mean TAC increase [%] |
| 3.2 | 6.38 | 6.40 | 5.38 | 6.89 | 0.3 |
| 2.8 | 6.39 | 6.45 | 5.93 | 6.92 | 0.9 |
| 2.4 | 6.41 | 6.54 | 6.09 | 6.97 | 2.0 |
| 2.0 | 6.47 | 6.67 | 6.30 | 7.07 | 3.1 |
| 1.6 | 6.55 | 6.86 | 6.57 | 7.23 | 4.7 |
| 1.2 | 6.68 | 7.12 | 6.90 | 7.43 | 6.6 |
| 0.8 | 6.88 | 7.47 | 7.31 | 7.72 | 8.6 |
| 0.4 | 7.25 | 8.06 | 8.00 | 8.21 | 11.2 |
| 0.0 | 8.10 | 9.37 | 9.37 | 9.37 | 15.7 |

provides a detailed view of energy balances in stochastic optimization, further highlighting the variability of the results.

### 3.3. Sensitivity to electricity demand

In addition to RES production, another major source of uncertainty in a HRES system is electricity demand. While an in-depth uncertainty characterization was not performed for this parameter, a sensitivity analysis was conducted considering initially two opposite scenarios:

1. A 10 % decrease in demand applied to all the hours of the year.
2. A 10 % increase in demand applied to all the hours of the year.

For each of these two additional scenarios, the same multi-objective optimization analysis described in Sections 3.1 and 3.2 was performed. Results are displayed in Fig. 12 and Table 7.

As illustrated in Fig. 9, the stochastic Pareto front exhibits a fan shape, reflecting the impact of uncertainty on both costs and emissions, due to the variable use of DGs. The same shape is found varying the electricity demand. However, in Fig. 12 the focus is placed on costs uncertainty, and consequently, data are positioned at the constraint level of $CO_2$ emissions. The key conclusions from the previous section remain valid even when the electricity demand varies. The stochastic analysis yields higher costs on average compared to the deterministic one. This discrepancy becomes more pronounced at lower emissions levels, since the system can not rely on DGs as flexible buffers. For the same reason, the variability in TACs across stochastic scenarios also diminishes as the constraint becomes stricter, as it is mainly driven by different levels of diesel purchase.

Although the trend remains the same, the impact of demand variation is significant. A decrease in demand shifts both deterministic and stochastic Pareto fronts toward lower costs, while an increase in demand shifts both fronts toward higher costs. Table 7 quantifies these variations, focusing on minimum TACs and zero-emissions scenarios. For stochastic optimization, average values are reported.

Interestingly, the percentage variation in TACs closely aligns with the ±10 % change in demand, for both deterministic and stochastic cases. The variation in system costs is, in fact, directly linked to the need for larger or smaller components to match changes in electricity demand. In particular, under the zero-emissions scenario, there is a monotonic increase in the size of all components as electricity demand increases. This trend is observed in both the deterministic and stochastic optimizations, as illustrated in Fig. 13. As the underlying optimization

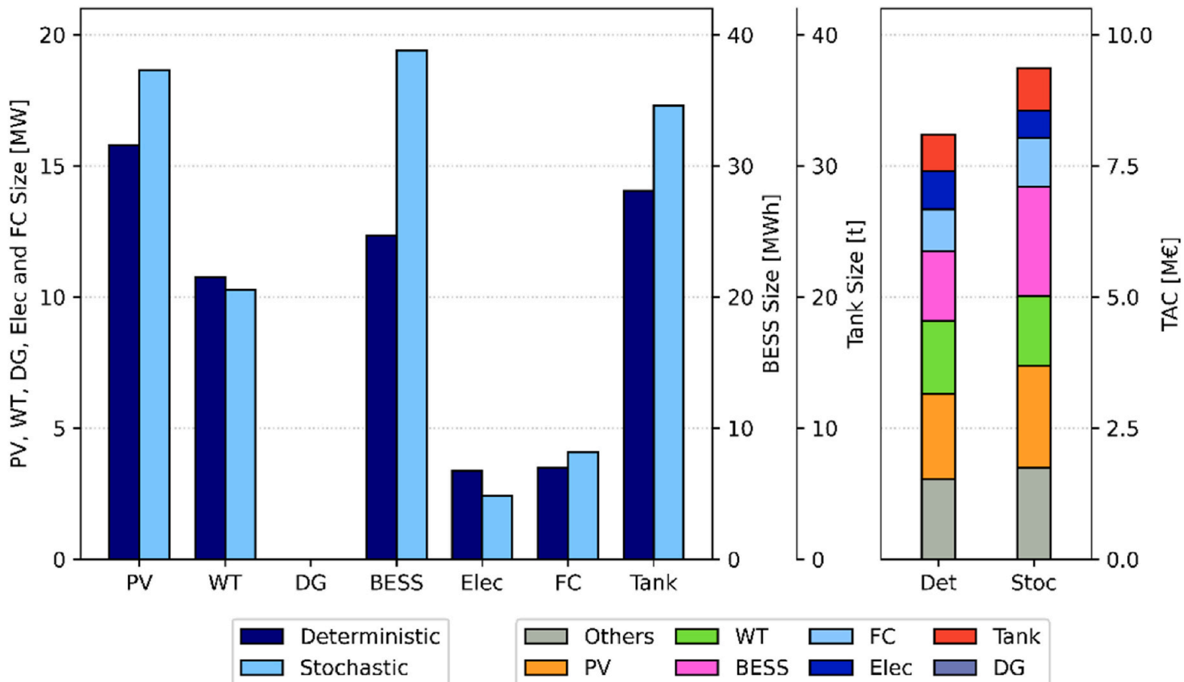


**Fig. 10.** Component sizes in deterministic and stochastic analyses for zero-emissions scenario (left) and their impact on TACs (right).

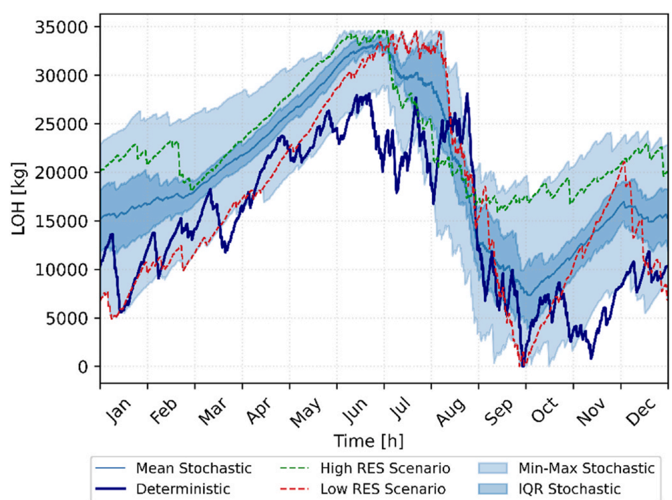


**Fig. 11.** Level of Hydrogen in deterministic and stochastic optimization for zero emissions configuration.

problem is linear, the system responds proportionally to a uniform and monotonic variation in electricity demand. Specifically, all the components scale by approximately the same percentage as demand increases. Since both CAPEX and OPEX – expressed as a percentage of CAPEX – are modeled as linear functions of capacity, the TACs also increase nearly linearly. A slight deviation from perfect proportionality occurs due to the minimum SOC constraint imposed on the battery, which leads to threshold effects by limiting the available energy. In general, more significant nonlinear behaviors could arise from nonlinear efficiency curves, or cost curves for some components, none of which can be present in an LP formulation. This linear trend persists even for larger variations in demand (e.g., +30 % and +50 %), as detailed in Appendix B.

Comparing the reference deterministic scenario to the most precautionary one – where demand increases by 10 % and stochastic optimization is applied – the effect of uncertainty integration becomes clear. The PV capacity increases from 15.8 MW to 20.5 MW (+29.7 %), while the wind turbine power sees a more moderate rise from 10.8 MW to 11.3 MW (+4.6 %). For storage systems, BESS capacity expands from 24.6 MWh to 42.7 MWh (+73.6 %), while hydrogen tank size grows from 28.1 t to 38.0 t (+35.2 %). These size variations result in a TACs increase of 27.0 %, from 8.10 M€ to 10.29 M€.

In case studies like the one presented in this paper, electricity demand is particularly prone to seasonal fluctuations, especially during the summer months when tourism activity peaks. To investigate this effect more accurately, an additional scenario was analyzed in which the 10 % demand increase was applied only from June to September. This adjustment results in an average annual demand increase of approximately 4.18 %. In the minimum TACs scenario, this seasonal demand increase led to a slight reduction in total annualized costs compared to the scenario where the demand increase was distributed across the entire year. For the deterministic case, TACs dropped from 7.00 M€ to

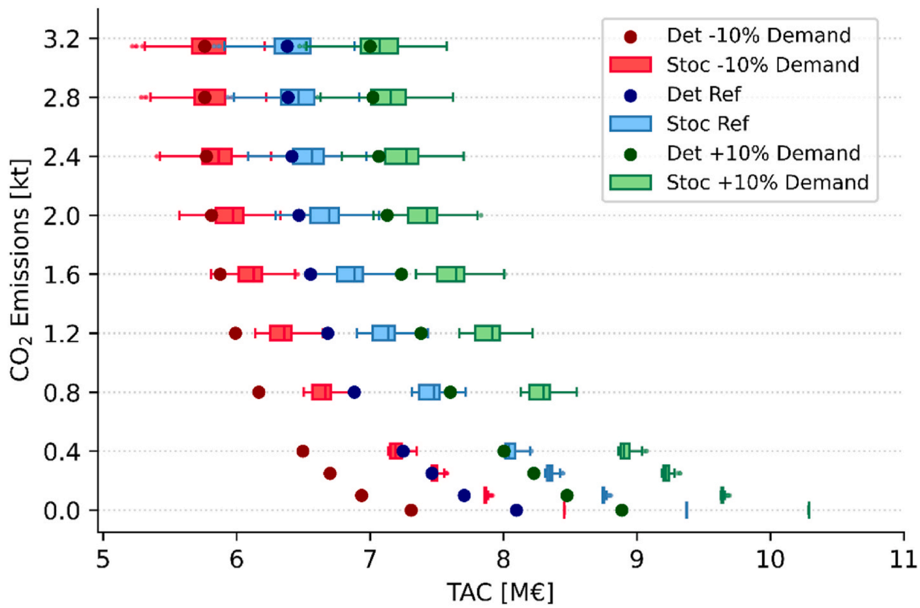


**Fig. 12.** Sensitivity to electricity demand - TACs at different $CO_2$ emissions for deterministic and stochastic analyses.

**Table 7**
TACs sensitivity to electricity demand in minimum TACs and zero-emissions configurations.

| Scenario | Zero-Emissions | | Minimum TACs | |
|---|---|---|---|---|
| | TACs [M€] | Variation [%] | TACs [M€] | Variation [%] |
| Det −10 % | 7.31 | −9.8 | 5.76 | −9.7 |
| Det Ref | 8.10 | – | 6.38 | – |
| Det +10 % | 8.89 | +9.8 | 7.00 | +9.7 |
| Stoc −10 % | 8.46 | −9.7 | 5.76 | −10.0 |
| Stoc Ref | 9.37 | – | 6.40 | – |
| Stoc +10 % | 10.29 | +9.8 | 7.06 | +10.3 |

6.77 M€, while in the stochastic case, they decreased from a mean of 7.06 M€ to 6.87 M€. This cost reduction can be attributed to the flexibility provided by the diesel generators, which, acting as dispatchable sources, allowed for a marginal downsizing of other system components, as the total demand to be covered is lower. However, when emissions constraints are imposed and diesel usage is eliminated, the difference in system costs between the summer-only and full-year demand increase scenarios becomes negligible. This outcome is explained by the alignment between peak demand and summer months: in the absence of dispatchable fossil-fuel sources, the system must be sized to meet peak load conditions using renewable and storage technologies alone. As a result, even a summer-only increase in demand leads to the same increase in the size of the components. Consequently, higher renewable energy curtailment is obtained during the rest of the year, particularly in the winter months. As shown in Fig. 14, curtailment in the deterministic case rises from 27.5 GWh (39.2 % of production) to 29.9 GWh (42.6 %) when demand is increased only during summer. Similar trends were observed in the stochastic optimization results.

This analysis highlights the added value of considering uncertainty in the HRES design process, as well as the cost implications of ensuring system reliability under variable renewable energy production and electricity demand.

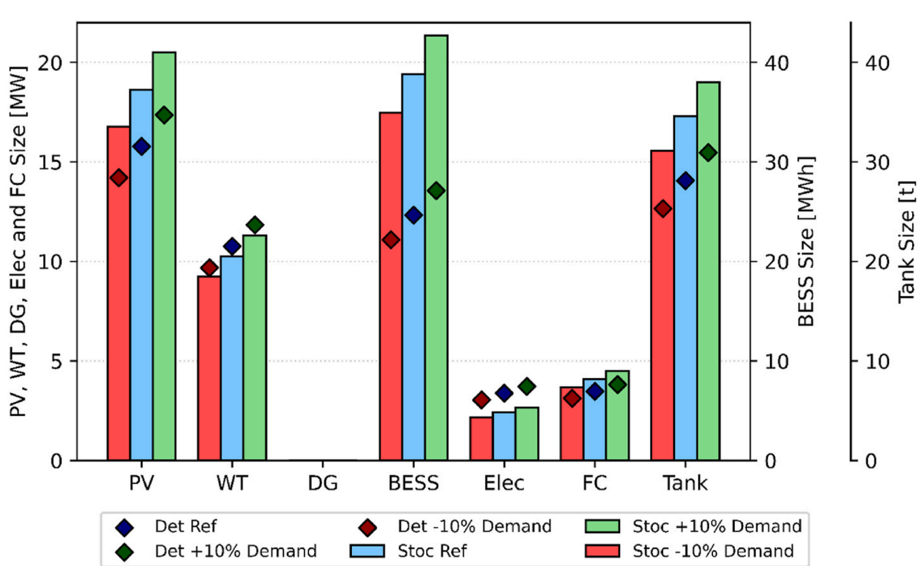


**Fig. 13.** Sensitivity to electricity demand – component sizes variation in deterministic and stochastic analyses.

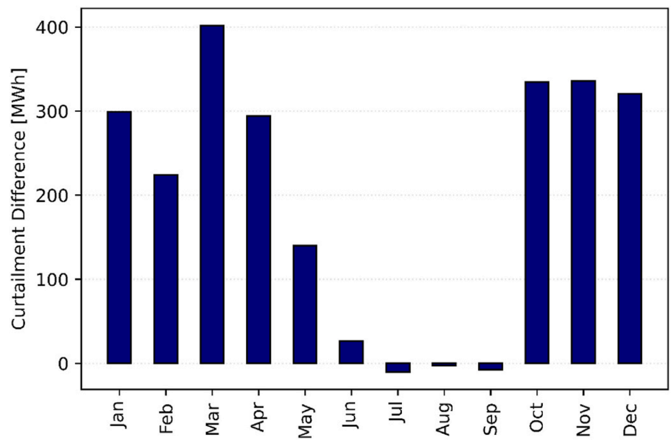


**Fig. 14.** Monthly difference in RES curtailment between the scenario with 10 % increased demand during summer months only (June–September) and the scenario with a uniform year-round 10 % increase.

## 4. Conclusions

This study presents a two-stage stochastic programming optimization framework to evaluate the impact of uncertainty on the sizing and operation of a Hybrid Renewable Energy System in remote areas. The methodology was applied to Pantelleria, an Italian island that relies on diesel generators for electricity production. The multi-objective optimization aimed at minimizing Total Annualized Costs and $CO_2$ emissions was conducted using an ε-constraint approach, allowing the identification of a Pareto front that illustrates the trade-off between cost and emissions reduction.

The deterministic analysis revealed that the most cost-effective configuration achieves a 58.8 % reduction in TACs compared to the current diesel-based scenario, demonstrating the economic viability of HRES. Additionally, this configuration also achieves an 86.5 % decrease in emissions, passing from an emission factor of 762 $g_{CO2}$/kWh to 103 $g_{CO2}$/kWh.

As the emissions constraint is tightened, component sizes increase to compensate for the loss of dispatchable diesel generation. This effect is particularly evident for storage systems, with BESS capacity increasing by 2.2 times and hydrogen tank capacity by 6.7 times in the zero-emissions scenario. The upscaling results in TACs rising from 6.38 M€ to 8.10 M€ (+27.0 %) in a fully renewable configuration. Despite this cost increase, the zero-emission scenario remains more cost-effective than the current diesel-based system (47.7 % TACs reduction), reinforcing the economic feasibility of a transition to renewables.

In the stochastic optimization, when the use of DGs remains possible, the component sizes are similar to the deterministic case, and the average TACs are comparable. However, high variability in TACs is observed due to the different use of diesel in the various scenarios. Conversely, when diesel generation is restricted or eliminated by emissions constraints, it is necessary to increase component sizes, particularly for storage systems. In the zero-emissions scenario, BESS capacity increases by 59.0 %, while hydrogen storage increases by 23.1 %, leading to a 15.7 % increase in mean TACs compared to the deterministic case. This result demonstrates that fully renewable systems must be sized more conservatively to ensure reliability under uncertain conditions.

The sensitivity analysis on electricity demand further confirms that higher energy demand necessitates larger system sizes and higher costs. The most precautionary scenario - which combines a 10 % increase in electricity demand with stochastic optimization - leads to a 27 % increase in TACs compared to the reference deterministic case in the fully renewable configuration.

The framework could be further improved by implementing an MILP approach, which would allow for a more detailed representation of operational constraints and discrete decision variables. While this approach would enhance the accuracy of results, it would also introduce a higher computational cost, in particular in stochastic optimization. Additionally, future research could explore the integration of thermal and transport energy sectors, providing a more comprehensive optimization of multi-energy systems and identifying the investment strategies required for a fully optimized energy transition.

The findings of this study reinforce the viability of renewable energy investments, demonstrating that the transition to a hybrid renewable configuration in isolated systems is economically competitive with the current diesel-based system. However, the introduction of stochastic optimization reveals the significant impact of uncertainty on system sizing and costs, underscoring the necessity of integrating uncertainty analysis into HRES design.

## CRediT authorship contribution statement

**Mattia Calabrese:** Writing – original draft, Software, Methodology, Investigation, Formal analysis, Conceptualization. **Andrea Ademollo:** Writing – review & editing, Software, Methodology, Investigation. **Carlo Carcasci:** Writing – review & editing, Supervision, Methodology.

## Data availability

Data will be made available on request.

## Funding

This research did not receive any specific grant from funding agencies in the public, commercial, or not-for-profit sectors.

## Declaration of competing interest

The authors declare that they have no known competing financial interests or personal relationships that could have appeared to influence the work reported in this paper.

## Appendix A

Figure A.1 reports the energy balances of the system in deterministic and stochastic optimization by representing the energy produced or consumed by each component. Data are aggregated on a daily basis for better visualization. The figure shows the high variability of the operation of the system across the scenarios.

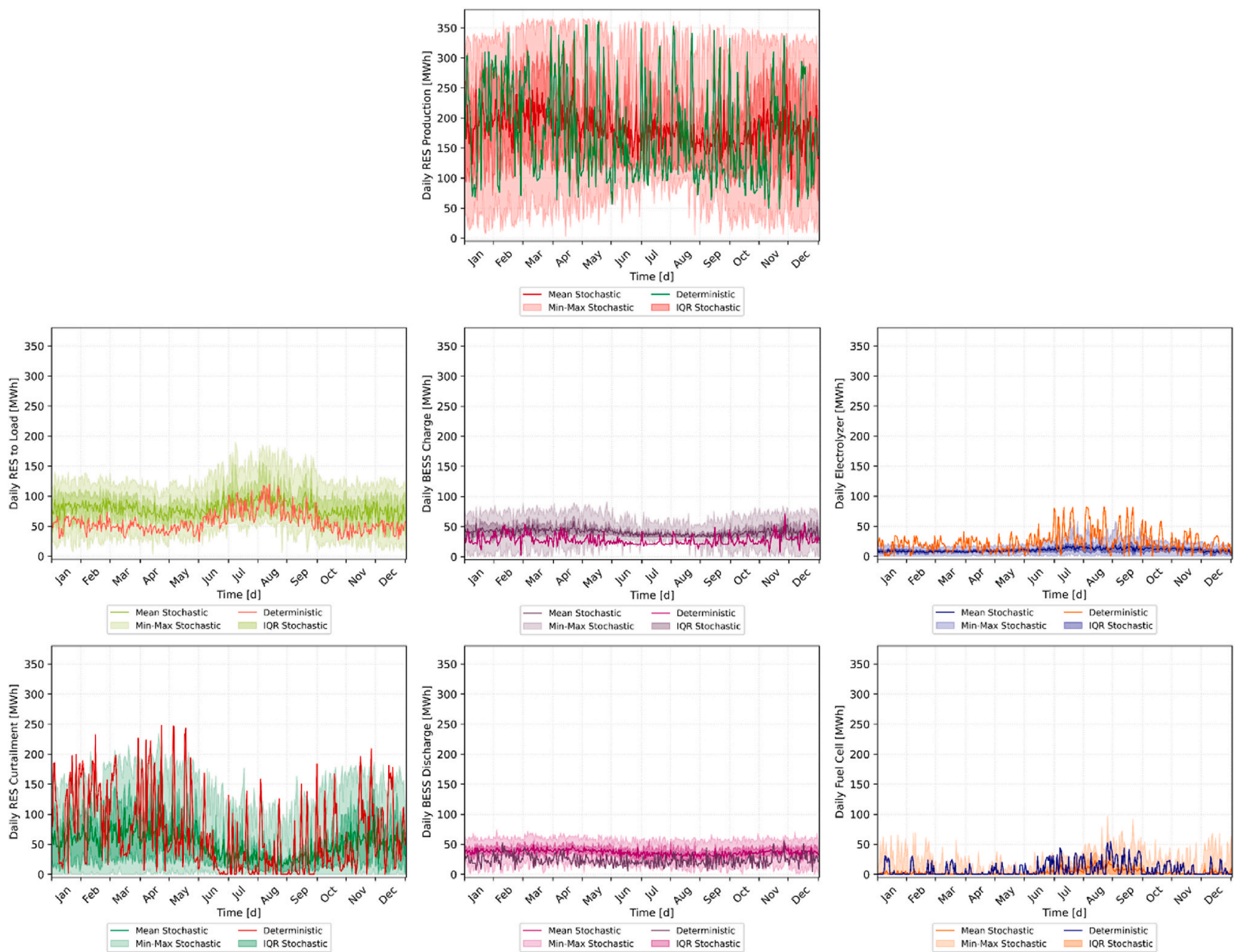


**Fig. A.1.** Daily energy production and consumption of different components in deterministic and stochastic analyses.

## Appendix B

To complement the sensitivity analysis presented in the main text, a further investigation was carried out to evaluate the impact of different variations in electricity demand, specifically by ±30 % and ±50 %. The objective was to assess whether the trend observed for a 10 % variation – namely, a proportional growth in component sizing and costs – persists. As shown in Figure B.1, both deterministic and stochastic optimizations result in a monotonic increase in TACs that closely follows the increase in electricity demand. This linear behavior is consistent across all demand levels analyzed. This trend suggests that the system scales coherently with demand increments.

Figure B.2, which reports the component sizes variation for the zero emissions scenario, further confirms that the capacity of the various technologies increases approximately in proportion to the demand levels, with no evident signs of nonlinear behavior even at ±50 % demand.

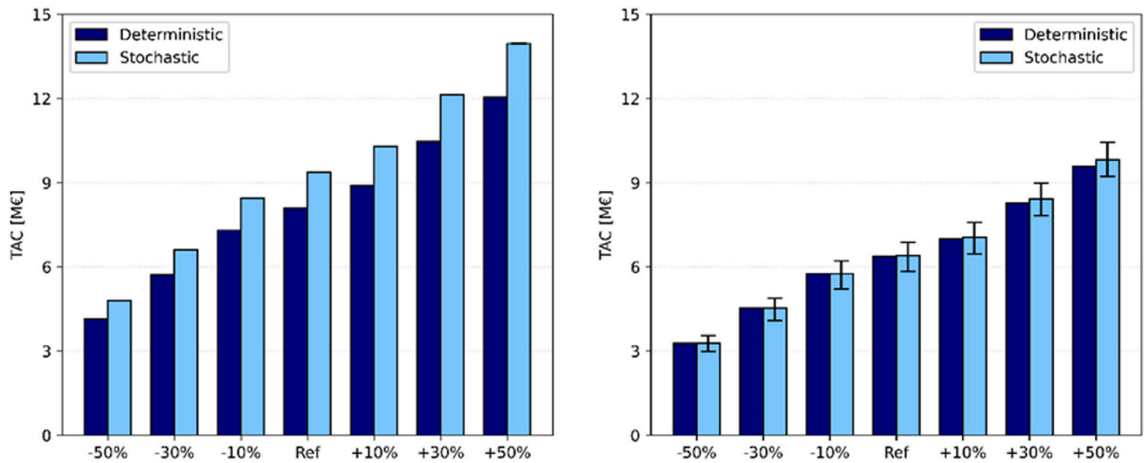


**Fig. B.1.** Comparison of TACs for deterministic and stochastic optimization under varying electricity demand levels in zero emissions (left) and minimum TACs (right) scenarios.

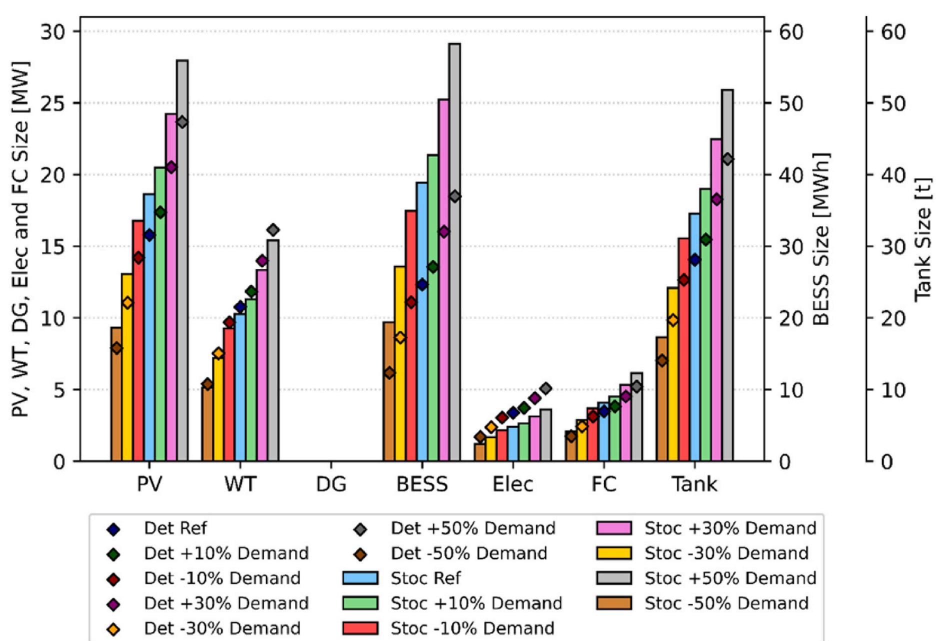


**Fig. B.2.** Sensitivity to electricity demand with ±10 %, 30 % and 50 % variation – component sizes variation in deterministic and stochastic analyses.

## Nomenclature

| Acronyms | | | |
|---|---|---|---|
| BESS | Battery Energy Storage System | MILP | Mixed Integer Linear Programming |
| CAPEX | Capital Expenditures | NREL | National Renewable Energy Laboratory |
| $CO_2$ | Carbon Dioxide | OPEX | Operating Expenditures |
| DEA | Danish Energy Agency | P2G2P | Power to Gas to Power |
| DG | Diesel Generator | PEM | Proton-Exchange Membrane |
| EU | European Union | PEMEL | PEM Electrolyzer |
| GHG | Greenhouse Gas | PEMFC | PEM Fuel Cell |
| HRES | Hybrid Renewable Energy System | PV | Photovoltaic |
| HSS | Hydrogen Storage System | PVGIS | Photovoltaic Geographical Information System |
| IEA | International Energy Agency | RES | Renewable Energy Sources |
| IQR | Interquartile Range | RSE | Italian agency for energy system research |
| LCOE | Levelized Cost of Electricity | SOC | State Of Charge |
| LHV | Lower Heating Value | TAC | Total Annualized Costs |
| LOH | Level Of Hydrogen | TOTEM | Territory Overview Tool for Energy Modelling |
| LP | Linear Programming | WT | Wind Turbine |
| MC | Monte Carlo | | |

| Symbols | Meanings | Units |
|---|---|---|
| $A$ | Annuity Factor | – |
| $C$ | Cost | € |
| $c$ | Cost Rate | – |
| $C-\ rate$ | Battery C-Rate | – |
| $Cap$ | Battery capacity | kWh |
| $CAPEX$ | Capital Expenditures | € |
| $dr$ | Real Discount Rate | – |
| $dr'$ | Nominal Discount Rate | – |
| $em$ | Emission Factor | $kg/m^3$ |
| $h$ | Height | m |
| $ir$ | Inflation Rate | – |
| $lt$ | Lifetime | – |
| $m$ | Mass flow rate | kg/h |
| $n$ | Number | – |
| $OPEX$ | Operating Expenditures | € |
| $P$ | Power | kW |
| $p$ | Probability | – |
| $QQ$ | Volumetric flow rate | $m^3/h$ |
| $R$ | Number of replacements | – |
| $S$ | Scenarios | – |
| $sc$ | Specific Cost | $€/m^3$ |
| $Size$ | Hydrogen tank size | kg |
| $TAC$ | Total Annualized Costs | € |
| $\boldsymbol{X}$ | Array of hourly energy output | – |
| $\boldsymbol{x}$ | Array of daily energy output | – |
| $t$ | Timestep | h |
| $v$ | Speed | m/s |
| $\alpha$ | Wind power law exponent | – |
| $\delta$ | Water consumption factor | $m^3/kg$ |
| $\mu$ | Cluster Centroid | kWh |
| $\varepsilon$ | Electrolyzer conversion efficiency | kWh/kg |
| $\zeta$ | Fuel Cell conversion efficiency | kg/kWh |
| $\eta$ | Efficiency | – |
| $\rho$ | Replacement Rate | – |
| $\varsigma$ | Specific energy production | $kWh/kW_p$ |
| $\sigma$ | Battery self-discharge rate | – |

| Subscripts | | | |
|---|---|---|---|
| BT | Battery | H2O | Water |
| ch | Charge | HT | Hydrogen Tank |
| ci | Cut-in | inst | Installation |
| CL | Cluster | inv | Investment |
| co | Cut-out | max | Maximum |
| CO | Compressor | MC | Monte Carlo |
| $CO_2$ | Carbon Dioxide | min | Minimum |
| CURT | Curtailment | O&M | Operation and Maintenance |
| DEM | Demand | pers | Personnel |
| diesel | Diesel | PV | Photovoltaic |
| dis | Discharge | r | Rated |
| DG | Diesel Generator | ref | Reference |
| EL | Electrolyzer | start | Start |
| end | End | target | Target |
| eng | Engineering | w | Wind |
| FC | Fuel Cell | WT | Wind Turbine |
| H2 | Hydrogen | y | Years |

## References


[1] IEA, Net zero by 2050 – analysis. https://www.iea.org/reports/net-zero-by-2050, 2021. (Accessed 31 January 2025).
[2] EU, Fit for 55 - the EU's plan for a green transition – consilium. https://www.consilium.europa.eu/en/policies/fit-for-55/. (Accessed 31 January 2025).
[3] IEA, CO2 emissions in 2022 – analysis. https://www.iea.org/reports/co2-emissions-in-2022, 2023. (Accessed 31 January 2025).
[4] IEA, Islands need resilient power systems more than ever. Clean Energy can Deliver – Analysis, 2024. https://www.iea.org/commentaries/islands-need-resilient-power-systems-more-than-ever-clean-energy-can-deliver. (Accessed 31 January 2025).
[5] EU Commissions, Clean energy vision to clean energy action | clean energy for EU islands. https://clean-energy-islands.ec.europa.eu/, 2025. (Accessed 31 January 2025).
[6] A. Malheiro, P.M. Castro, R.M. Lima, A. Estanqueiro, Integrated sizing and scheduling of wind/PV/diesel/battery isolated systems, Renew. Energy 83 (2015) 646–657, https://doi.org/10.1016/J.RENENE.2015.04.066.
[7] W. Cai, X. Li, A. Maleki, F. Pourfayaz, M.A. Rosen, M. Alhuyi Nazari, D.T. Bui, Optimal sizing and location based on economic parameters for an off-grid application of a hybrid system with photovoltaic, battery and diesel technology, Energy 201 (2020) 117480, https://doi.org/10.1016/J.ENERGY.2020.117480.
[8] P. Marocco, D. Ferrero, A. Lanzini, M. Santarelli, Optimal design of stand-alone solutions based on RES + hydrogen storage feeding off-grid communities, Energy Convers. Manag. 238 (2021) 114147, https://doi.org/10.1016/J.ENCONMAN.2021.114147.
[9] E.M. Gray, C.J. Webb, J. Andrews, B. Shabani, P.J. Tsai, S.L.I. Chan, Hydrogen storage for off-grid power supply, Int. J. Hydrogen Energy 36 (2011) 654–663, https://doi.org/10.1016/J.IJHYDENE.2010.09.051.
[10] M. Brinkhaus, D. Jarosch, J. Kapischke, All year power supply with off-grid photovoltaic system and clean seasonal power storage, Sol. Energy 85 (2011) 2488–2496, https://doi.org/10.1016/J.SOLENER.2011.07.007.
[11] P. Marocco, D. Ferrero, A. Lanzini, M. Santarelli, The role of hydrogen in the optimal design of off-grid hybrid renewable energy systems, J. Energy Storage 46 (2022) 103893, https://doi.org/10.1016/J.EST.2021.103893.
[12] O.V. Marchenko, S.V. Solomin, Modeling of hydrogen and electrical energy storages in wind/PV energy system on the Lake Baikal coast, Int. J. Hydrogen Energy 42 (2017) 9361–9370, https://doi.org/10.1016/J.IJHYDENE.2017.02.076.
[13] H. Borhanazad, S. Mekhilef, V. Gounder Ganapathy, M. Modiri-Delshad, A. Mirtaheri, Optimization of micro-grid system using MOPSO, Renew. Energy 71 (2014) 295–306, https://doi.org/10.1016/J.RENENE.2014.05.006.
[14] M.S. Mahbub, D. Viesi, S. Cattani, L. Crema, An innovative multi-objective optimization approach for long-term energy planning, Appl. Energy 208 (2017) 1487–1504, https://doi.org/10.1016/J.APENERGY.2017.08.245.
[15] M.S. Mahbub, D. Viesi, L. Crema, Designing optimized energy scenarios for an Italian alpine valley: the case of giudicarie esteriori, Energy 116 (2016) 236–249, https://doi.org/10.1016/J.ENERGY.2016.09.090.
[16] T. Tezer, R. Yaman, G. Yaman, Evaluation of approaches used for optimization of stand-alone hybrid renewable energy systems, Renew. Sustain. Energy Rev. 73 (2017) 840–853, https://doi.org/10.1016/J.RSER.2017.01.118.
[17] A. Ademollo, M. Calabrese, C. Carcasci, An up-to-date perspective of levelized cost of hydrogen for PV-based grid-connected power-to-hydrogen plants across all Italy, Appl. Energy 379 (2025) 124958, https://doi.org/10.1016/J.APENERGY.2024.124958.
[18] M. Vaccari, G.M. Mancuso, J. Riccardi, M. Cantù, G. Pannocchia, A sequential linear programming algorithm for economic optimization of hybrid renewable energy systems, J. Process Control 74 (2019) 189–201, https://doi.org/10.1016/J.JPROCONT.2017.08.015.
[19] P. Marocco, D. Ferrero, E. Martelli, M. Santarelli, A. Lanzini, An MILP approach for the optimal design of renewable battery-hydrogen energy systems for off-grid insular communities, Energy Convers. Manag. 245 (2021) 114564, https://doi.org/10.1016/J.ENCONMAN.2021.114564.
[20] R. Dufo-López, I.R. Cristóbal-Monreal, J.M. Yusta, Stochastic-heuristic methodology for the optimisation of components and control variables of PV-wind-diesel-battery stand-alone systems, Renew. Energy 99 (2016) 919–935, https://doi.org/10.1016/J.RENENE.2016.07.069.
[21] Y. Gong, T. Liu, P. Liu, L. Duan, Flexible operation space of hydro–hydrogen–based hybrid power systems, Renew. Sustain. Energy Rev. 209 (2025) 115114, https://doi.org/10.1016/J.RSER.2024.115114.
[22] E. Marzi, M. Morini, C. Saletti, S. Vouros, V. Zaccaria, K. Kyprianidis, A. Gambarotta, Power-to-Gas for energy system flexibility under uncertainty in demand, production and price, Energy 284 (2023) 129212, https://doi.org/10.1016/j.energy.2023.129212.
[23] Y.H. Huang, J.H. Wu, Y.J. Hsu, Two-stage stochastic programming model for the regional-scale electricity planning under demand uncertainty, Energy 116 (2016) 1145–1157, https://doi.org/10.1016/J.ENERGY.2016.09.112.
[24] MIUR, Smart island EU, (n.d.). http://www.smartisland.eu/(accessed January 31, 2025).
[25] D. Lauinger, P. Caliandro, J. Van herle, D. Kuhn, A linear programming approach to the optimization of residential energy systems, J. Energy Storage 7 (2016) 24–37, https://doi.org/10.1016/J.EST.2016.04.009.
[26] P. Gabrielli, M. Gazzani, M. Mazzotti, Electrochemical conversion technologies for optimal design of decentralized multi-energy systems: modeling framework and technology assessment, Appl. Energy 221 (2018) 557–575, https://doi.org/10.1016/J.APENERGY.2018.03.149.
[27] G. Mavrotas, Effective implementation of the ε-constraint method in multi-objective mathematical programming problems, Appl. Math. Comput. 213 (2009) 455–465, https://doi.org/10.1016/j.amc.2009.03.037.
[28] L. Li, J. Wang, X. Zhong, J. Lin, N. Wu, Z. Zhang, C. Meng, X. Wang, N. Shah, N. Brandon, S. Xie, Y. Zhao, Combined multi-objective optimization and agent-based modeling for a 100% renewable island energy system considering power-to-gas technology and extreme weather conditions, Appl. Energy 308 (2022) 118376, https://doi.org/10.1016/j.apenergy.2021.118376.
[29] EU Commission, JRC photovoltaic geographical information system (PVGIS). https://re.jrc.ec.europa.eu/pvg_tools/en/. (Accessed 31 January 2025).
[30] RSE, Aeolian. https://atlanteeolico.rse-web.it/. (Accessed 31 January 2025).
[31] K.M. Simmons, D. Sutter, Tornado warnings, lead times, and tornado casualties: an empirical investigation, Weather Forecast. 23 (2008) 246–258, https://doi.org/10.1175/2007WAF2006027.1.
[32] L. Moretti, M. Astolfi, C. Vergara, E. Macchi, J.I. Pérez-Arriaga, G. Manzolini, A design and dispatch optimization algorithm based on mixed integer linear programming for rural electrification, Appl. Energy 233–234 (2019) 1104–1121, https://doi.org/10.1016/J.APENERGY.2018.09.194.
[33] Danish Energy Agency, Technology data for energy storage. https://ens.dk/en/analyses-and-statistics/technology-data-energy-storage. (Accessed 31 January 2025).
[34] L. Gracia, P. Casero, C. Bourasseau, A. Chabert, Use of hydrogen in off-grid locations, a techno-economic assessment, Energies 11 (2018) 3141, https://doi.org/10.3390/EN11113141, 2018, Vol. 11, Page 3141.
[35] W. Cole, A. Karmakar, Cost projections for utility-scale battery storage: 2023 update. https://doi.org/10.2172/1984976, 2023.
[36] A. Ademollo, A. Mati, M. Pagliai, C. Carcasci, Exploring the role of hydrogen in decarbonizing energy-intensive industries: a techno-economic analysis of a solid oxide fuel cell cogeneration system, J. Clean. Prod. 469 (2024) 143254, https://doi.org/10.1016/J.JCLEPRO.2024.143254.
[37] A. Singlitico, J. Østergaard, S. Chatzivasileiadis, Onshore, offshore or in-turbine electrolysis? techno-economic overview of alternative integration designs for green hydrogen production into offshore wind power hubs, Renew. Sustain. Energy Transit. 1 (2021) 100005, https://doi.org/10.1016/J.RSET.2021.100005.
[38] Danish Energy Agency, Technology data for renewable fuels. https://ens.dk/en/analyses-and-statistics/technology-data-renewable-fuels. (Accessed 31 January 2025).
[39] Danish Energy Agency, Technology data for generation of electricity and district heating. https://ens.dk/en/analyses-and-statistics/technology-data-generation-electricity-and-district-heating. (Accessed 31 January 2025).
[40] IEA, Technology roadmap - hydrogen and fuel cells. https://www.iea.org/reports/technology-roadmap-hydrogen-and-fuel-cells. (Accessed 31 January 2025).
[41] Tractebel and Hinicio, Study on early business cases for H2 in energy storage and more broadly power to H2 applications. https://www.h2knowledgecentre.com/content/researchpaper1130, 2017. (Accessed 31 January 2025).
[42] A.Q. Jakhrani, A.R.H. Rigit, A.K. Othman, S.R. Samo, S.A. Kamboh, Estimation of carbon footprints from diesel generator emissions, in: Proceedings of the 2012 International Conference in Green and Ubiquitous Technology, GUT, 2012, pp. 78–81, https://doi.org/10.1109/GUT.2012.6344193, 2012.
[43] M.K. Deshmukh, S.S. Deshmukh, Modeling of hybrid renewable energy systems, Renew. Sustain. Energy Rev. 12 (2008) 235–249, https://doi.org/10.1016/J.RSER.2006.07.011.
[44] P. Marocco, D. Ferrero, A. Lanzini, M. Santarelli, Optimal design of stand-alone solutions based on RES + hydrogen storage feeding off-grid communities, Energy Convers. Manag. 238 (2021) 114147, https://doi.org/10.1016/J.ENCONMAN.2021.114147.
[45] P. Nikolaidis, A. Poullikkas, A comparative overview of hydrogen production processes, Renew. Sustain. Energy Rev. 67 (2017) 597–611, https://doi.org/10.1016/J.RSER.2016.09.044.
[46] P. Marocco, K. Sundseth, T. Aarhaug, A. Lanzini, M. Santarelli, A.O. Barnett, M. Thomassen, Online measurements of fluoride ions in proton exchange membrane water electrolysis through ion chromatography, J. Power Sources 483 (2021) 229179, https://doi.org/10.1016/J.JPOWSOUR.2020.229179.
[47] E. Crespi, G. Luca, M. Testi, C. Maggi, V. Bona, M.B. Barone, G. Staffetti, L. Crema, Renewable hydrogen production through electrolysis: an analysis of the cost gap for its economic competitiveness in Italy, Int. J. Hydrogen Energy 68 (2024) 1163–1177, https://doi.org/10.1016/J.IJHYDENE.2024.04.303.
[48] Corporate Finance Institute, Fisher equation - overview, formula and example. https://corporatefinanceinstitute.com/resources/economics/fisher-equation/. (Accessed 31 January 2025).
[49] P. Marocco, D. Ferrero, M. Gandiglio, M.M. Ortiz, K. Sundseth, A. Lanzini, M. Santarelli, A study of the techno-economic feasibility of H2-based energy storage systems in remote areas, Energy Convers. Manag. 211 (2020) 112768, https://doi.org/10.1016/J.ENCONMAN.2020.112768.
[50] Trading Economics, Euro area inflation rate. https://tradingeconomics.com/euro-area/inflation-cpi. (Accessed 31 January 2025).
[51] IEA-PVPS, National survey reports archive. https://iea-pvps.org/national-survey-reports, 2022. (Accessed 31 January 2025).
[52] NREL, Utility-scale PV. https://atb.nrel.gov/electricity/2024/utility-scale_pv, 2024. (Accessed 31 January 2025).
[53] NREL, Land-based wind. https://atb.nrel.gov/electricity/2024/land-based_wind, 2024. (Accessed 31 January 2025).
[54] NREL, Utility-scale battery storage. https://atb.nrel.gov/electricity/2024/utility-scale_battery_storage, 2024. (Accessed 31 January 2025).

[55] European hydrogen observatory, electrolyser cost. https://observatory.clean-hydrogen.europa.eu/hydrogen-landscape/production-trade-and-cost/electrolyser-cost, 2024. (Accessed 31 January 2025).
[56] M. Yang, R. Hunger, S. Berrettoni, B. Sprecher, B. Wang, A review of hydrogen storage and transport technologies, Clean Energy 7 (2023) 190–216, https://doi.org/10.1093/CE/ZKAD021.
[57] J. Brandt, T. Iversen, C. Eckert, F. Peterssen, B. Bensmann, A. Bensmann, M. Beer, H. Weyer, R. Hanke-Rauschenbach, Cost and competitiveness of green hydrogen and the effects of the European Union regulatory framework, Nat. Energy 9 (2024) 703–713, https://doi.org/10.1038/s41560-024-01511-z.
[58] EU Commission, Pantelleria - clean energy for EU islands. https://clean-energy-islands.ec.europa.eu/countries/italy/pantelleria. (Accessed 31 January 2025).
[59] S.G. Simoes, J. Catarino, A. Picado, T.F. Lopes, S. di Berardino, F. Amorim, F. Gírio, C.M. Rangel, T. Ponce de Leão, Water availability and water usage solutions for electrolysis in hydrogen production, J. Clean. Prod. 315 (2021) 128124, https://doi.org/10.1016/J.JCLEPRO.2021.128124.
[60] RSE, TOTEM. https://totem.rse-web.it/. (Accessed 31 January 2025).
[61] H. Li, Z. Ren, M. Fan, W. Li, Y. Xu, Y. Jiang, W. Xia, A review of scenario analysis methods in planning and operation of modern power systems: methodologies, applications, and challenges, Elec. Power Syst. Res. 205 (2022) 107722, https://doi.org/10.1016/J.EPSR.2021.107722.
[62] P. Tapetado, J. Usaola, Capacity credits of wind and solar generation: the Spanish case, Renew. Energy 143 (2019) 164–175, https://doi.org/10.1016/J.RENENE.2019.04.139.
[63] N.Y. Krakauer, D.S. Cohan, Interannual variability and seasonal predictability of wind and solar resources, Resources 6 (2017) 29, https://doi.org/10.3390/RESOURCES6030029, 2017, Vol. 6, Page 29.
[64] Electricity Map, Live 24/7 $CO_2$ emissions of electricity consumption. https://app.electricitymaps.com/map/72h/hourly. (Accessed 31 March 2025).